identify the type of *bcr–abl* mutations present in imatinib-resistant patients.

For these reasons, mutation testing should be performed to ensure the successful therapeutic management of CML and Ph$^+$ALL patients. Various techniques have been developed to detect mutations. Direct Sequencing (DS) is widely used but is cumbersome, time-consuming and of low sensitivity (detection limit is around 25%) [9]. Several alternative methods have been reported, such as D-HPLC [10], allele-specific oligonucleotide PCR (ASO-PCR) [11], pyrosequencing [12] and peptide nucleic acid (PNA)-based PCR clamping [13]. These methods are more sensitive than DS. However, they are not easily automated. We previously developed a fully integrated and automated point mutation detection method using quenching probes (QP method) to detect the JAK2V617F mutation associated with myeloproliferative neoplasms at higher sensitivity around 3% [14]. We adapted the QP method to enable detection of frequently observed *bcr–abl* mutations which were clinically very relevant in imatinib-resistant patients. Furthermore, we developed a more sensitive method, mutation-biased PCR-QP (MBP-QP), which is 10 times more sensitive than the original QP method, in order to specifically detect the T315I clone. In the present study, we validated the QP and MBP-QP methods with peripheral blood samples obtained from imatinib-resistant patients.

2. Materials and methods

2.1. Patients

This study was reviewed and approved by the Institutional Review Board of Kyoto University Hospital and all patients provided informed consent before the collection of bone marrow or peripheral blood samples in accordance with the Declaration of Helsinki. In each patient, one peripheral blood sample was collected and analysed at the time when a patient was diagnosed as failure or suboptimal response to imatinib. Patients with a failed or suboptimal response to imatinib treatment were defined according to the European Leukemia Net (ELN) criteria [15]. Patient characteristics are summarized in Table 1.

2.2. Plasmids expressing mutated bcr–abl and human CML cell lines

abl fragments containing a mutated amino acid region for each different mutation were amplified by PCR using genomic DNA as a template and subcloned into the pT7Blue T-Vector (Novagen, San Diego, CA, USA). All the mutations (M244V, G250E, Q252H, Y253F, Y253H, E255K, E255V, V299L (G895C), V299L (G895T) T315A, T315I, F317L, M351T, E355G, F359V, F359C, and H396R) were produced using the QuickChange II Site-Directed Mutagenesis Kit™ (Stratagene, La Jolla, CA) and confirmed by DS.

2.3. QP method

This study was conducted using a fully automated single nucleotide polymorphism (SNP) detection system (prototype i-densy™, ARKRAY Inc., Kyoto, Japan). Details of this machine and the principles underlying the QP method have been described previously [14]. Prototype i-densy™ (Supplementary Fig. 1) comprises three parts: a pre-treatment cartridge, a reagent cartridge and an amplification/detection tube. The method automatically performs pre-treatment, DNA amplification, and mutation detection via melting temperature (Tm) analysis. Briefly, whole blood (100 μL) was applied to the pre-treatment cartridge and the system was started. A primer (Supplementary Table 1)/probe (Supplementary Table 2) mix and an enzyme mix (each dispensed in separate wells in advance) were mixed in the amplification/detection tube, and competitive oligonucleotides (Supplementary Table 1), which bind PCR products from wild-type *abl*, were added to the reagent cartridge to improve the sensitivity. The compositions of reaction mixes (primer/probe) for the different mutations are summarized in Supplementary Table 3. The lid of the tube catches a reaction chip in the pre-treatment cartridge and the FTA™ (Whatman, Tokyo, Japan), which captures and stabilizes the DNA on the tip of the reaction chip, were soaked into the applied whole blood. After washing three times to eliminate any factors in the blood that may inhibit amplification, the FTA was added to the tube containing the mixed reagents and DNA amplification begun. The amplification conditions used were: 50 cycles of 1 s at 95 °C and 30 s (15 s for V299L) at the annealing temperature. After DNA amplification, Tm analysis using a guanine-quenching probe (QProbe) was utilized to detect the mutations. The total fluorescence generated by the QProbe bound complementarily to each target sequence and the melting curves generated by Tm analysis were then used to identify fluorescence quenching. All steps were completed within 90 min.

Table 1
Patient characteristics.

		Total	CML-CP	CML-AP	CML-BC	Ph$^+$ALL
		131	97	6	11	17
Age (year) at diagnosis	Median	49	57	45	45	34
	Range	3–84	6–84	6–63	3–77	6–71
Gender	Male	77	57	3	7	10
	Female	54	40	3	4	7
Mutation status	Mutation	32	17	4	4	7
	No mutation	99	80	2	7	10

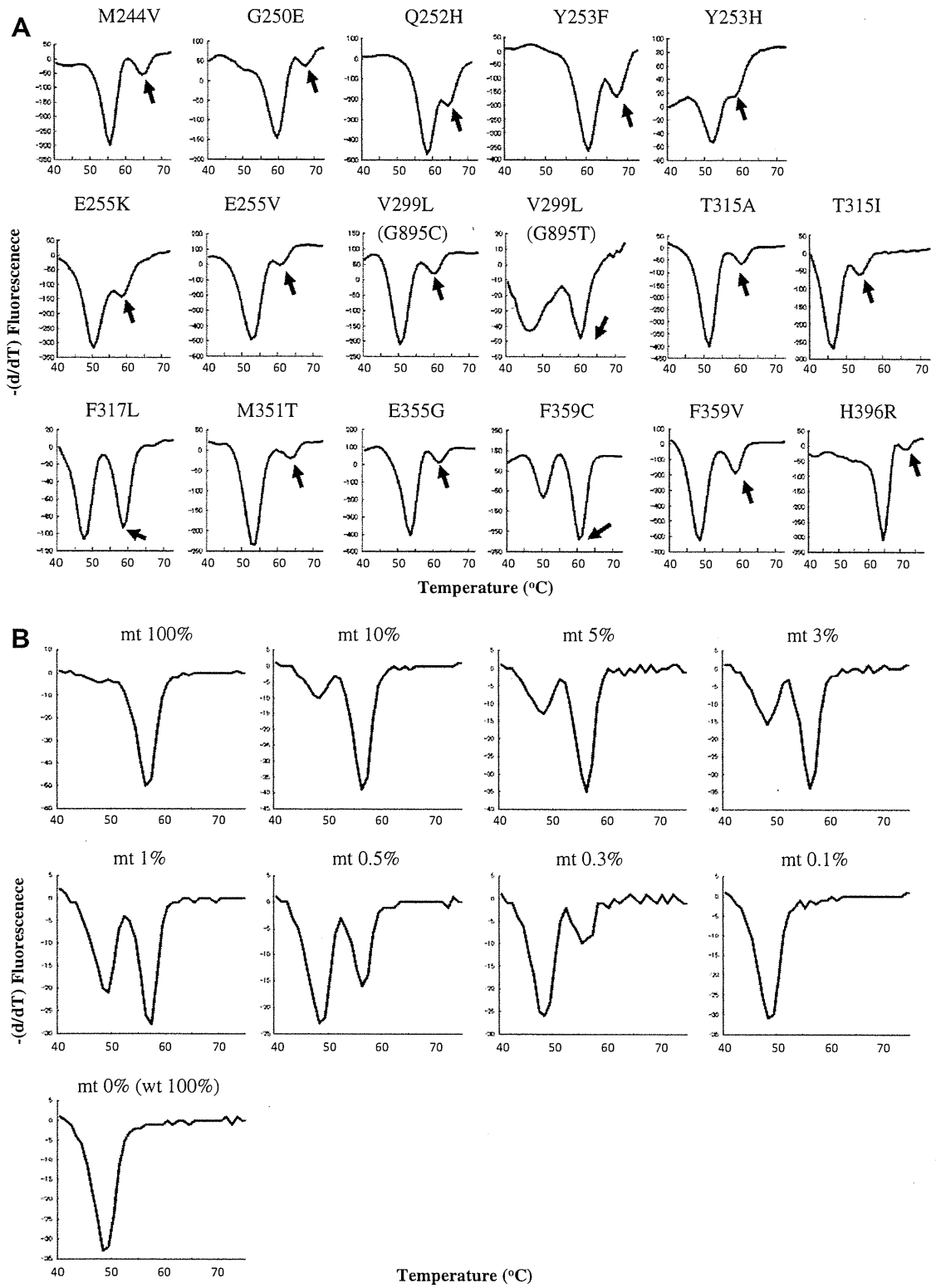

Fig. 1. Sensitivity of the QP and MBP-QP method for *bcr–abl* mutations. (A) Melting curves of the sample which contained wild type and each of the 17 kinds of mutated clones at 97.5% and 2.5%, respectively. Arrows indicate the peaks which suggest the existence of each mutated clone. All mutations evaluated herein can be detected at least 3% sensitivity. (B) Melting curves of each concentration of T315I clones. Arrows indicate the peaks which suggest the existence of each mutated clone. A peak which indicated for T315I was obvious at 0.3%, while it was not obvious at 0.1%, suggesting that the high-sensitivity (MBP-QP) method had a detection limit of 0.3%.

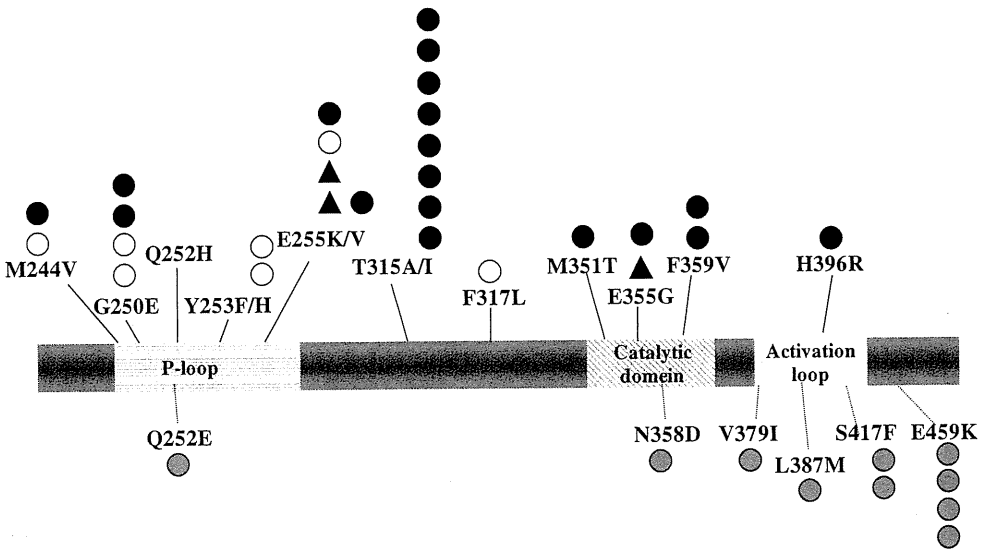

Fig. 2. Comparison between the QP system and DS for the detection of imatinib-resistant related mutations. The results which mutations were detected by both methods (QP and DS) and which mutations could be detected by either of the two are indicated by as follows; QP positive and DS positive (●), QP positive and DS negative (▲), QP negative because of out of setting and DS positive (◍), QP negative even though within our setting and DS positive (○).

2.4. MBP-QP method

Because of the clinical significance of T315I (it is resistant to all currently available second generation ABL TKIs), the QP method was refined to yield higher sensitivity. To obtain amplicons from mutant alleles, the PCR step within the QP method was redesigned. The primers used to detect the wild-type and T315I sequences were of different lengths, which lead to more efficient amplification of the mutant sequences. All other steps were as described for the original QP method.

2.5. RNA extraction, cDNA synthesis, and RT-PCR for direct sequencing

Total RNA was extracted from peripheral blood or bone marrow cells using a QIAmp RNA blood mini kit (Qiagen, Tokyo, Japan) according to the manufacturer's instructions. Reverse transcription was performed using a High Capacity cDNA Reverse Transcription Kit (Applied Biosystems, Tokyo, Japan). BCR–ABL fusion transcripts were amplified by PCR using primers specific for *bcr* and *abl*.

2.6. Direct Sequencing (DS)

DS was performed in parallel with the QP method to confirm the results. After PCR amplification, the *bcr–abl* cDNA transcripts were sequenced using a BigDye Terminator Cycle Sequencing kit (Applied Biosystems) and an ABI3130XL sequencer (Applied Biosystems). The mutant sequences were compared with the wild-type sequences using DNASIS. All analyses were performed by BML Co., Ltd., Tokyo, Japan.

3. Results

3.1. Sensitivity of the QP and MBP-QP method

The sensitivity of the QP method for *bcr–abl* mutations was tested using graded mixes of plasmids containing both wild-type and mutated sequences. The mixes ranged from 1% to 100% mutated oligonucleotides in the following ratios (% mutant:% wild type): 100:0, 50:50, 30:70, 20:80, 10:90, 5:95, 2.5:97.5, and 1:99. To ensure reproducibility, the plasmid mix synthesized from each stock solution was tested in triplicate in the QP method.

The melting curves are shown in Fig. 1A and the mutant-specific peak is indicated by an arrow in each case. The data indicated that the QP method had a detection limit for mutations below 3%, which indicated that a *bcr–abl* mutation could be detected at least approximately, e.g. 1–3% depending on the specific mutant in the mutant: wild-type mixture. By contrast, DS was only able to detect mutations at >20% in this method (data not shown). Each probe was set for the detection of each mutation. In a case of multiple mutations in one patient, the mutations were not demonstrated in one wave. For example, if a patient's leukemic cells harbored two mutations such as E255K and T315I, the results which indicated these mutations were obtained from two waves which revealed the existence of E255K and T315I clone, respectively.

Modification of the PCR step by incorporating primers of different lengths to detect the wild-type and T315I sequences (MBP-QP; which enables more effective amplification of mutated PCR products) resulted in increased sensitivity for T315I, with a detection limit of 0.3% (Fig. 1B).

3.2. Patient characteristics and frequency of mutations

In total, 131/133 samples yielded comparable results using the two different detection methods, QP and DS. Samples from two patients (1.5%) were discarded due to poor RNA quality. At the time of failure or suboptimal response to imatinib, 97 patients were in CP, 6 in AP, 5 in myeloid BC, one in biphenotypic BC, 5 in lymphoid BC, and 17 had Ph^+ALL (Table 1). Thirty-two patients harbored 38 *bcr–abl* mutations comprising 17 different types. These were identified by either method in 17/97 (17.5%) CML-CP, 4/6 (66.7%) CML-AP, and 11/28 (39.3%) CML-BC/Ph^+ALL patients (Table 1).

3.3. Comparison of QP and DS in imatinib-resistant patients

The QP method was able to detect the p-loop mutations M244 V ($n = 1$), G250E ($n = 2$), E255K ($n = 3$) and E255V ($n = 1$), the imatinib-binding domain mutation T315I ($n = 8$), the catalytic domain mutations

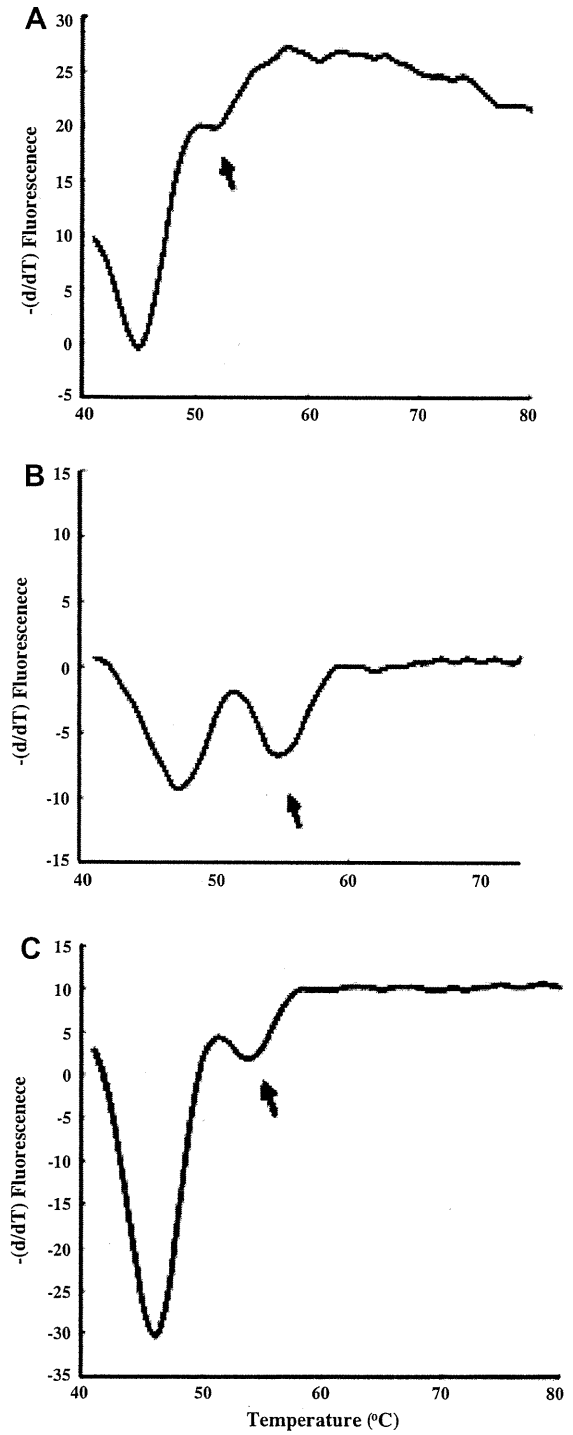

Fig. 3. Detection of T315I using the high sensitivity MBP-QP method. (A) A melting curve obtained by the original QP method of peripheral blood taken from an imatinib resistant patient showed only a very faint peak at higher temperature which indicated the existence of a T315I clone. In addition, DS could not detect the T315I at this point. (B) A melting curve obtained by MBP-QP method of the same sample revealed the obvious peak at higher temperature which indicated the existence of a T315I clone, indicating that MBP-QP was more sensitive than the original QP method. (C) A melting curve obtained by the original QP method of the same sample after 1 month clearly detected the T315I, indicating that the MBP-QP method detected T315I 1 month earlier than the original QP method.

M351T ($n = 1$), E355G ($n = 2$), F359V ($n = 2$), and the activation-loop mutation, H396R ($n = 1$) (Fig. 2). 18/37 in positive cases was concordance with the results of QP and DS. Three positive mutations (E255K/V: $n = 2$, and E355G: $n = 1$) showed that the QP method was effective. In particular, the most serious mutation, T315I, was with complete correspondence. However, only DS detected 17 cases, the QP method was not set up to detect some *bcr–abl* mutations (e.g., Q252E, N358D, V379I, L387M, S417F, and E459K). E459K mutation was detected more than expected, and likely to be added to the setting mutations. It still did not detect five mutations that it was set up for (e.g., G250E, M244V, Y253H, E255K and F317L) in seven cases. This is the example of false negative and needed to enhance sensitivity in combination with MBP-QP.

3.4. Comparison of the MBP-QP method for T315I versus DS in imatinib-resistant patients

The high sensitivity MBP-QP method was used to detect T315I mutations. In total, 52 samples were comparable using MBP-QP and the original QP method. MBP-QP detected seven positive samples, whereas the original QP method detected only three. The positive samples from four patients might express minimal levels of the T315I clone. The details of four cases in which only the more sensitive MBP-QP method was able to detect the T315I at low levels were as follows; In the first case, MBP-QP detected the T315I mutation at the early stage of the disease, when only the wild type was detected by DS and the original QP method. However, after 1 month, the original QP method clearly detected the T315I, indicating that the MBP-QP method detected T315I 1 month earlier than the original QP method (Fig. 3). In the second CML-CP case, no progression was observed with imatinib at least for half year after the detection of T315I by only MBP-QP. Unfortunately, further mutation analyses were not performed because of drop out from the clinical study. Thus, it was currently unclear whether a small population of T315I clone detected by MBP-QP affected the prognosis of the patients. The third case which was diagnosed as Ph$^+$ALL had a hematopoietic stem cell transplantation (HSCT) after the emergence of T315I mutation by MBP-QP. After HSCT, the patient sustained complete remission and no mutations have been detected. The firth case diagnosed Ph$^+$ALL whose leukemic cells harbored not only T315I detected by MBP-QP but also E255K detected by the original QP method also had a HSCT. Unfortunately, we could not analyze the mutation status because of early death after HSCT.

4. Discussion

Despite the successful use of imatinib to treat many CML and Ph$^+$ALL patients with mutated BCR–ABL clones, some show only partial responses or fail to respond at all [16]. This indicated that not all mutations at ABL KD are clinically very relevant. Although DS is commonly used to detect mutations, its sensitivity is usually around 20–25% [9], which may be insufficient for optimal treatment of CML and Ph$^+$ALL patients. In addition, DS is also a time-consuming and labor-intensive method.

In this study, we describe the development of a simple, automated assay for the detection of frequently observed *bcr–abl* point mutations that were clinically relevant. This method consists of a PCR amplification step and a Tm analysis step that uses a quenching probe. Mutations were detected in 17 CML-CP patients (17.5%) and our data support a previous study that identified differences in the relevant mutations in each disease phase (Table 1 and Fig. 2) [16]. In particular, the most serious mutation, T315I, was frequently identified in CML-BC and Ph$^+$ALL patients (Fig. 2). T315I mutations are associated with poor clinical outcomes for patients with CML-BC and Ph$^+$ALL [17]. Interestingly, disease progression did not occur in one CML-CP patient identified as having the T315I by MBP-QP in the present study, and the number of BCR–

ABL mRNA copies was maintained at a steady level by treatment with imatinib (data not shown). However, in one patient with CML-BC, we predicted disease progression by detecting the presence of T315I (Fig. 3). Our results are consistent with those of other reports showing that the survival of patients harboring T315I is dependent on the phase of the disease [17], and suggest that MBP-QP for T315I may facilitate the decision to treat with TKIs or with stem cell transplantation, especially in cases of CML-AP/BC and Ph^+ALL. A prospective study using the MBP-QP method to identify T315I in dasatinib-treated patients is currently underway.

In the present study, minor mutations outside our settings were detected more frequently than expected (Fig. 2). Minor and novel mutations have been reported for other ethnic groups, e.g., South Koreans (S417Y, E450K, E459K, and P480L) [18], Chinese (I418V, E450A, E453L, and E455K) [19], and French (L298L, Y320C, L324Q, F359L, and F376L) [20]. Further investigation is needed to understand the significance of these novel mutations in a clinical setting. However, it is highly possible that these mutations do not affect the efficacy of other TKIs; in the case of E459K, for example, bosutinib binds to the active conformation of BCR–ABL [21]. All second generation ABL TKIs, such as dasatinib, nilotinib, bosutinib and bafetinib, can eliminate most mutations; however, there are slight differences in their sensitivity to each mutation [7,8]. For example, dasatinib is effective against Y253F/H and F359C/V, which cannot be eliminated by nilotinib. On the other hand, dasatinib is ineffective against F317L, V299L and Q253H, which are sensitive to nilotinib [16]. Thus, the appropriate combination of ABL TKIs can be used to eliminate most mutant clones, except T315I. Moreover, in the post-imatinib era, it may not be necessary to detect all imatinib-resistant related mutations. It may be sufficient to test for several mutations that have low sensitivity to second generation ABL TKIs. Therefore, we are constructing the mutation packages for the nilotinib setting (T315A, V299L, F317L/V/I/C) and the dasatinib one (E255K/V, Y253H, or F359V/I/C).

Thus, the QP method that cannot detect low-frequency mutations may play a more active part in the management of Ph^+ leukemia patients. However, this method can help determine the management of the second TKIs especially in de novo CML patients.

As described, the QP method may become a useful tool in clinic for the detection of *bcr–abl* mutations. In the cases of QP positive/DS negative, there may be doubt that QP method leads false positive. However, we think that there is little possibility according to the following reasons. Concerning the possible false-positive data obtained by QP method, it may be the best way to check all the data (QP positive/DS negative) by the allele specific PCR (ASO-PCR). We have previously reported that QP method can avoid false positivity in the case of JAK2V617F mutation [14]. We confirmed the accuracy of data obtained by QP method with ASO-PCR on JAK2V617F. In addition, theoretically, there is little possibility of false-positivity by QP method. The Tm analysis in QP method is based on the hydrogen bonding between quenching probes and PCR products after the PCR amplification step. This step is simply the physical reaction and there is little possibility of the inappropriate binding of quenching probe to the amplified PCR product. Even though of little possibility, assuming that QP method reveals the false-positive, it is due to the error in PCR amplification step. It is much lower that the lacking of proofreading activity rates such as *Taq* DNA polymerase (less than 2.6×10^{-5}). Thus, it is little possibility that an identical point mutation which is detected by quenching probe is accumulated by PCR reaction because of miss proofreading.

However, the QP method is not perfect to detect mutations in TKI-resistant patients since it can detect only already-known mutations for which appropriate primer/probe combinations have been prepared. Thus, by design of our study, the QP method could not detect mutations Q252E, N358D, V379I, L387M, S417F and E459K which were not so frequently observed in imatinib resistant patients. Another drawback of the QP method is the process of PCR. When we analysed *bcr–abl* mutations using DS, only cDNA derived from the fusion transcript of *bcr–abl* were used. In contrast, detection of *bcr–abl* mutations with the QP method is based on extraction of, "genomic" DNA from peripheral blood and contained *abl* fragments from both leukemic cells and normal cells was used for the detection of *bcr–abl* mutations. To reduce the influence of *abl* fragments from normal cells, the competitive oligonucleotides were added to the system (Supplementary Table 1). With this contrivance, the QP method has superior performance than DS for the detection of *bcr–abl* mutations. However, the QP method failed to detect mutations that were detected by DS in seven cases (Fig. 2) even though the primer/probe combinations were designed for those mutations. A possible explanation for this finding is a deficiency of the competitive oligonucleotides. These problems may be resolved by the MBP-QP which in the present study was adapted to detect the T315I mutation.

In conclusion, because of its convenience and speed, the QP method is useful in clinical laboratories in that it facilitates therapy decisions for patients treated with ABL TKIs. Moreover the MBP-QP method may become the more important method for mutation detection because of its greater sensitivity. Since the QP method can be adapted to detect any mutation merely by changing the PCR primers and QProbes used, it may become a very useful adjunct to personalized medicine in which treatment decisions will increasingly be based on detection of specific mutations. Examples include the rapid detection of EGFR mutations in lung cancer, of c-KIT mutations in gastrointestinal stromal tumor and KRAS mutations in colon cancer.

Conflict of interest

None declared.

Acknowledgements

We thank Naoko Hashimoto and Mikiko Katakami for technical support. We would also like to thank Jun Kuroki,

Atsushi Kitabayashi, Hisako Iso, Hideyoshi Noji and Hideo Kimura, and all the various clinical centres participating in this study. This work was partly supported by Grant-in-Aids for Scientific Research and for the Japan Society for the Promotion of Science (JSPS) fellows, by the Global COE Program "Centre for Frontier Medicine" from the Ministry of Education, Culture, Sports, Science and Technology (MEXT) of Japan, and by Management Expenses Grants from the Government to the National Cancer Centre of Japan.

Appendix A. Supplementary material

Supplementary data associated with this article can be found, in the online version, at doi:10.1016/j.canlet.2011.08.009.

References

[1] J.M. Goldman, J.V. Melo, Chronic myeloid leukemia – advances in biology and new approaches to treatment, N. Engl. J. Med. 349 (2003) 1451–1464.
[2] F. Gruber, S. Mustjoki, K. Porkka, Impact of tyrosine kinase inhibitors on patient outcomes in Philadelphia chromosome-positive acute lymphoblastic leukaemia, Br. J. Haematol. 145 (2009) 581–597.
[3] E. Weisberg, P.W. Manley, S.W. Cowan-Jacob, A. Hochhaus, J.D. Griffin, Second generation inhibitors of BCR–ABL for the treatment of imatinib-resistant chronic myeloid leukaemia, Nat. Rev. Cancer 7 (2007) 345–356.
[4] J.F. Apperley, Part I: mechanisms of resistance to imatinib in chronic myeloid leukaemia, Lancet Oncol. 8 (2007) 1018–1029.
[5] R. Tanaka, S. Kimura, Abl tyrosine kinase inhibitors for overriding Bcr–Abl/T315I: from the second to third generation, Expert Rev. Anticancer Ther. 8 (2008) 1387–1398.
[6] T. O'Hare, C.A. Eide, M.W. Deininger, Bcr–Abl kinase domain mutations, drug resistance, and the road to a cure for chronic myeloid leukemia, Blood 110 (2007) 2242–2249.
[7] Y. Deguchi, S. Kimura, E. Ashihara, T. Niwa, K. Hodohara, Y. Fujiyama, T. Maekawa, Comparison of imatinib, dasatinib, nilotinib and INNO-406 in imatinib-resistant cell lines, Leukemia Res. 32 (2008) 980–983.
[8] S. Redaelli, R. Piazza, R. Rostagno, V. Magistroni, P. Perini, M. Marega, C. Gambacorti-Passerini, F. Boschelli, Activity of bosutinib, dasatinib, and nilotinib against 18 imatinib-resistant BCR/ABL mutants, J. Clin. Oncol. 27 (2009) 469–471.
[9] A.M. Vannucchi, A. Pancrazzi, C. Bogani, E. Antonioli, P. Guglielmelli, A quantitative assay for *JAK2* ^{V617F} mutation in myeloproliferative disorders by ARMS-PCR and capillary electrophoresis, Leukemia 20 (2006) 1055–1060.
[10] S. Soverini, G. Martinelli, M. Amabile, A. Poerio, M. Bianchini, G. Rosti, F. Pane, G. Saglio, M. Baccarani, Italian cooperative study group on chronic myeloid leukemia; European LeukemiaNet-6th framework program of the European community, denaturing-HPLC-based assay for detection of ABL mutations in chronic myeloid leukemia patients resistant to imatinib, Clin. Chem. 50 (2004) 1205–1213.
[11] F.X. Gruber, T. Lamark, A. Anonli, M.A. Sovershaev, M. Olsen, T. Gedde-Dahl, H. Hjort-Hansen, B. Skogen, Selecting and deselecting imatinib-resistant clones, observations made by longitudinal, quantitative monitoring of mutated BCR–ABL, Leukemia 19 (2005) 2159–2165.
[12] J.S. Khorashad, M. Anand, D. Marin, S. Saunders, T. Al-Jabary, A. Iqbal, S. Margerison, J.V. Melo, J.M. Goldman, J.F. Apperley, J. Kaeda, The presence of a BCR–ABL mutant allele in CML does not always explain clinical resistance to imatinib, Leukemia 20 (2006) 658–663.
[13] K.A. Kreuzer, P. le Coutre, O. Landt, I.K. Na, M. Schwarz, K. Schultheis, A. Hochhaus, B. Dörken, Preexistence and evolution of imatinib mesylate-resistant clones in chronic myelogenous leukemia detected by a PNA-based PCR clamping technique, Ann. Hematol. 82 (2003) 284–289.
[14] R. Tanaka, J. Kuroda, W. Stevenson, E. Ashihara, T. Ishikawa, T. Taki, Y. Kobayashi, Y. Kamitsuji, E. Kawata, M. Takeuchi, Y. Murotani, A. Yokota, M. Hirai, S. Majima, M. Taniwaki, T. Maekawa, S. Kimura, Fully automated and super-rapid system for the detection of JAK2V617F mutation, Leukemia Res. 32 (2008) 1462–1467.
[15] M. Baccarani, G. Saglio, J. Goldman, A. Hochhaus, B. Simonsson, F. Appelbaum, J. Apperley, F. Cervantes, J. Cortes, M. Deininger, A. Gratwohl, F. Guilhot, M. Horowitz, T. Hughes, H. Kantarjian, R. Larson, D. Niederwieser, R. Silver, R. Hehlmann, European LeukemiaNet, evolving concepts in the management of chronic myeloid leukemia: recommendations from an expert panel on behalf of the European LeukemiaNet, Blood 108 (2006) 1809–1820.
[16] S. Branford, J.V. Melo, T.P. Hughes, Selecting optimal second-line tyrosine kinase inhibitor therapy for chronic myeloid leukemia patients after imatinib failure: does the BCR–ABL mutation status really matter?, Blood 114 (2009) 5426–5435
[17] F.E. Nicolini, M.J. Mauro, G. Martinelli, D.W. Kim, S. Soverini, M.C. Müller, A. Hochhaus, J. Cortes, C. Chuah, I.H. Dufva, J.F. Apperley, F. Yagasaki, J.D. Pearson, S. Peter, C. Sanz Rodriguez, C. Preudhomme, F. Giles, J.M. Goldman, W. Zhou, Epidemiologic study on survival of chronic myeloid leukemia and Ph(+) acute lymphoblastic leukemia patients with BCR–ABL T315I mutation, Blood 114 (2009) 5271–5278.
[18] S.H. Kim, D. Kim, D.W. Kim, H.G. Goh, S.E. Jang, J. Lee, W.S. Kim, I.Y. Kweon, S.H. Park, Analysis of Bcr–Abl kinase domain mutations in Korean chronic myeloid leukaemia patients: poor clinical outcome of P-loop and T315I mutation is disease phase dependent, Hematol. Oncol. 27 (2009) 190–197 Y.
[19] Qin, S. Chen, B. Jiang, Q. Jiang, H. Jiang, J. Li, L. Li, Y. Lai, Y. Liu, X. Huang, Characteristics of BCR–ABL kinase domain point mutations in Chinese imatinib-resistant chronic myeloid leukemia patients, Ann. Hematol. 90 (2011) 47–52.
[20] F.E. Nicolini, S. Corm, O.H. Lê, N. Sorel, S. Hayette, D. Bories, T. Leguay, L. Roy, S. Giraudier, M. Tulliez, T. Facon, F.X. Mahon, J.M. Cayuela, P. Rousselot, M. Michallet, C. Preudhomme, F. Guilhot, C. Roche-Lestienne, Mutation status and clinical outcome of 89 imatinib mesylate-resistant chronic myelogenous leukemia patients: a retrospective analysis from the French intergroup of CML (Fi(phi)-LMC GROUP), Leukemia 20 (2006) 1061–1066.
[21] D. Kim, D.W. Kim, B.S. Cho, H.G. Goh, S.H. Kim, W.S. Kim, J. Lee, I.Y. Kweon, S.H. Park, J.H. Yoon, N.D. Kim, H. Chun, Structural modeling of V299L and E459K Bcr–Abl mutation, and sequential therapy of tyrosine kinase inhibitors for the compound mutations, Leukemia Res. 33 (2009) 1260–1265.

Cancer Science
The official journal of the Japanese Cancer Association

Rakicidin A effectively induces apoptosis in hypoxia adapted Bcr-Abl positive leukemic cells

Miki Takeuchi,[1,2] Eishi Ashihara,[1,3,6,7] Yohko Yamazaki,[4] Shinya Kimura,[5] Yoko Nakagawa,[1] Ruriko Tanaka,[1] Hisayuki Yao,[1] Rina Nagao,[1] Yoshihiro Hayashi,[1,2] Hideyo Hirai[1] and Taira Maekawa[1]

[1]Department of Transfusion Medicine and Cell Therapy, Kyoto University Hospital, Kyoto; [2]Division of Gastroenterology and Hematology, Department of Internal Medicine, Shiga University of Medical Science, Shiga; [3]Department of Molecular Cell Physiology, Kyoto Prefectural University of Medicine, Kyoto; [4]Institute of Microbial Chemistry, Numazu; [5]Division of Hematology, Respiratory Diseases and Oncology, Faculty of Medicine, Saga University, Saga, Japan

(Received October 12, 2010/Accepted November 23, 2010/Accepted manuscript online November 27, 2010/Article first published online December 19, 2010)

Treatment with Abl tyrosine kinase inhibitors (TKI) drastically improves the prognosis of chronic myelogenous leukemia (CML) patients. However, quiescent CML cells are insensitive to TKI and can lead to relapse of the disease. Thus, research is needed to elucidate the properties of these quiescent CML cells, including their microenvironment, in order to effectively target them. Hypoxia is known to be a common feature of solid tumors that contributes to therapeutic resistance. Leukemic cells are also able to survive and proliferate in severely hypoxic environments. The hypoxic conditions in the bone marrow (BM) allow leukemic cells that reside there to become insensitive to cell death stimuli. To target leukemic cells in hypoxic conditions, we focused on the hypoxia-selective cytotoxin, Rakicidin A. A previous report showed that Rakicidin A, a natural product produced by the *Micromonospora* strain, induced hypoxia-selective cytotoxicity in solid tumors. Here, we describe Rakicidin A-induced cell death in hypoxia-adapted (HA)-CML cells with stem cell-like characteristics. Interestingly, apoptosis was induced via caspase-dependent and -independent pathways. In addition, treatment with Rakicidin A in combination with the TKI, imatinib, resulted in synergistic cytotoxicity against HA-CML cells. In conclusion, Rakicidin A is a promising compound for targeting TKI-resistant quiescent CML stem cells in the hypoxic BM environment. (*Cancer Sci* 2011; 102: 591–596)

In solid tumors, oxygen supply is frequently insufficient to adequately support rapid cell proliferation and angiogenesis, which leads to the development of hypoxic regions within the tumor.[1,2] These hypoxic regions are associated with altered cell metabolism, changes in cell cycling and increased resistance to cell death stimuli, and are often associated with a poor prognosis in cancer patients.[3–5] Therefore, the development of cytotoxic compounds that are effective in hypoxic conditions might overcome the therapeutic resistance of cancer cells in hypoxic micro environments.

Bone marrow (BM) is known to have low levels of oxygen, and it has been suggested that the hematopoietic stem cells in the BM niche are protected from DNA damage induced by reactive oxygen species (ROS).[6,7] Chronic myelogenous leukemia (CML) is a disorder of hematopoietic stem cells caused by the constitutive activation of Bcr-Abl tyrosine kinase.[8] Treatment of CML has been markedly improved by the development of Abl tyrosine kinase inhibitors (TKI), but the complete eradication of CML cells may not be possible with TKI alone because they are largely ineffective against quiescent CML cells.[9–12] Although it has not yet been confirmed, CML stem cells could reside in the BM niche because they exhibit characteristics similar to normal hematopoietic stem cells. Previously, we found that CML cells engrafted in the BM survived and proliferated in the severely hypoxic environment; furthermore, these hypoxia-adapted leukemic cells acquired a more primitive phenotype.[13]

Recently, Yamazaki *et al.* screened 20 000 cultured broths of microorganisms and isolated Rakicidin A, a highly hypoxia-selective cytotoxic compound from *Micromonospora* strain ML99-43F1. Rakicidin A showed significant selective cell-killing effects in solid cancer cell lines.[14] In this study, Rakicidin A inhibited the proliferation of TKI-resistant, hypoxia-adapted CML (HA-CML) cells by inducing apoptosis. These findings indicate that hypoxia-selective therapy may be a novel strategy for the treatment of CML, especially Abl TKI-resistant quiescent CML cells.

Materials and Methods

Cell lines and reagents. The human CML derived cell line K562 was obtained from the American Type Culture Collection (Manassas, VA, USA) and KCL22 cells were kindly provided by Dr Tadashi Nagai (Jichi Medical School, Tochigi, Japan). The CML cell lines were maintained in RPMI-1640 supplemented with 10% fetal calf serum (Vitromex, Miami, FL, USA) at 37°C in a humidified atmosphere of 20% O_2, 5% CO_2 and 75% N_2. K562-HA and KCL22-HA cells were cultured continuously in 1.0% O_2 (7.2 mmHg), 5% CO_2 and 94% N_2.[13] Rakicidin A was synthesized and purified as described previously.[14] Imatinib and dasatinib were purchased from a pharmacy. zVAD was purchased from the Peptide Institute (Osaka, Japan). Imatinib, dasatinib, Rakicidin A and zVAD were dissolved in dimethyl sulfoxide and stored at −20°C until required for use. zVAD was used at 50 μM. The cells were preincubated with zVAD for 90 min.

Cell death. Cell viability was measured by the incorporation of propidium iodide (PI). Cells were seeded in a flat-bottomed 48-well plate at a concentration of 1.5×10^5 cells in 300 μL medium in each well and incubated with various concentrations of imatinib, dasatinib or Rakicidin A for 48 h. The mean of three measurements at each concentration was calculated. The IC_{50} values were obtained using the nonlinear regression program CalcuSyn (Biosoft, Cambridge, UK). We also evaluated the combined effects of concurrent Rakicidin A and imatinib treatment on both CML and HA-CML cells and their parental cells, and the results are presented as the combination index (CI). The CI is a method for quantifying drug cytotoxic synergism based on the mass-action law principle derived from enzyme kinetic models.[15,16] Cells were incubated for 48 h with six concentrations (0.25, 0.5, 0.75, 1.0, 1.5 or 2.0 times the IC_{50}) of each agent or both in combination, and the cytotoxic effect

[6]To whom correspondence should be addressed.
E-mail: ash0325@kuhp.kyoto-u.ac.jp
[7]Present address: Department of Molecular Cell Physiology, Kyoto Prefectural University of Medicine, Kyoto, Japan.

doi: 10.1111/j.1349-7006.2010.01813.x
© 2010 Japanese Cancer Association

was measured by PI staining. The CI was calculated as described previously,[17] and the fraction affected (Fa) was calculated at each dilution (i.e. an Fa of 0.25 would correspond to 75% viable cells). This method provides quantification of the synergism (CI <1), additive effect (CI = 1) and antagonistic effect (CI >1) at different dose and effect levels.

Colony-forming cell (CFC) assays. Bone marrow cells from two normal volunteers and CML patients in the chronic phase before imatinib treatment were purchased from AllCells Inc. (Emeryville, CA, USA). Thawed normal cells (2×10^4) and CML cells (1×10^4) were exposed to Rakicidin A, 0.25 μM, and 0.125 and 0.25 μM, respectively. A 0.1 mL volume of these cells was added to 1 mL standard methylcellulose culture medium (MethoCult 04435; StemCell Technologies, Vancouver, BC, Canada) and cultured for 14 days in 20% O_2 or 1% O_2. The numbers of CFC were counted under inverted microscopy (Olympus, Tokyo, Japan). Two dishes per treatment were evaluated.

Apoptosis and cell cycle analysis. The mitochondrial transmembrane potential ($\Delta\psi m$) was determined by staining with 3,3′-dihexyloxacarbocyanine iodide ($DiOC_6$; Molecular Probes, Eugene, OR, USA), as described previously.[18] For analysis of DNA content, the cells were fixed with ice-cold 70% ethanol and then incubated with propidium iodide (PI), as described previously.[19] The percentage of cells that incorporated PI, the $\Delta\psi m$ and the number of cells in the $subG_1$ phase of the cell cycle were determined using Facs Diva software (Becton Dickinson, San Jose, CA, USA) and ModiFit-LT software (Becton Dickinson). DNA fragmentation was analysed with the Flow-TACS Apoptosis Detection kit (Trevigen, Gaithersburg, MD, USA).

Morphologic evaluation by light microscopy. K562-HA cells were treated with 0.25 μM Rakicidin A for 12 h, and then subjected to cytospin and stained using a Diff-Quick kit (International Reagents, Kobe, Japan) before examination by light microscopy.

Measurement of caspase activity. Caspase-3 activities in untreated cells or cells treated with 0.25 μM Rakicidin A were measured using a Caspase Fluorometric Protease assay kit (MBL, Tokyo, Japan), as described previously.[18,20]

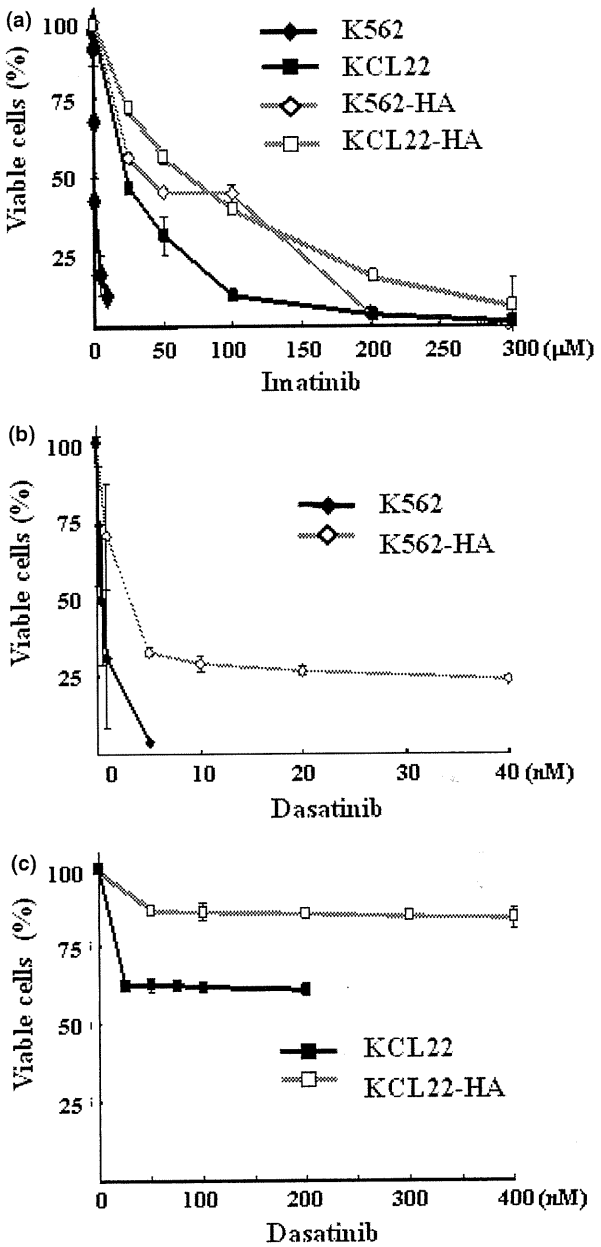

Fig. 1. Tyrosine kinase inhibitors (TKI) resistance induced by hypoxia-adapted chronic myelogenous leukemia (CML) cells *in vitro*. The CML cell lines K562 and KCL22 were subjected to continuous culture in 1.0% oxygen, and hypoxia-adapted subclones of K562-HA and KCL22-HA were selected. These hypoxia-adapted cells were maintained in suspension in low-oxygen conditions for more than 6 months. The cytotoxic effects of the indicated concentrations of imatinib against (a) parental K562 (closed diamond), parental KCL22 (closed square), K562-HA (open diamond) and KCL22-HA (open square) are shown. The cytotoxic effects of dasatinib against (b) parental K562 (closed diamond) and K562-HA (open diamond), and (c) parental KCL22 (closed square) and KCL22-HA (open square) are shown.

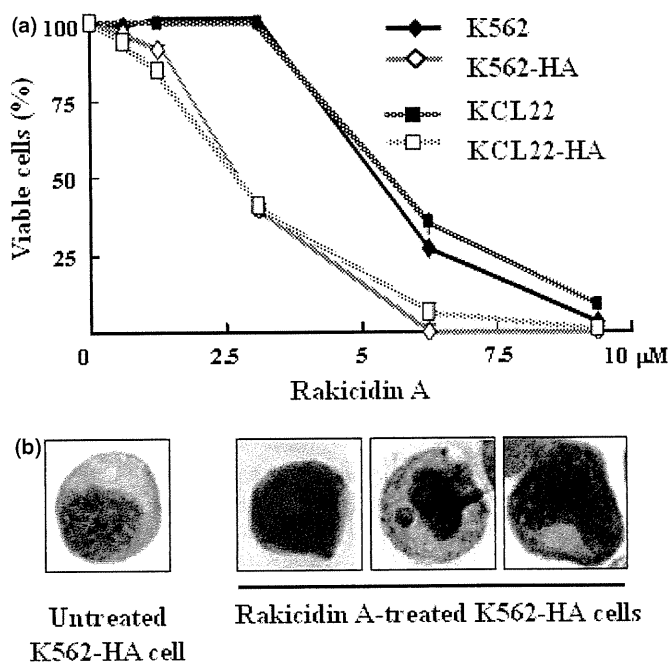

Fig. 2. Hypoxia-selective cell death inducing effects of Rakicidin A. Effect of Rakicidin A on hypoxia-adapted chronic myelogenous leukemia (HA-CML) cells. *In vitro* cytotoxic effects of Rakicidin A against (a) parental K562 (closed diamond), parental KCL22 (closed square), K562/HA (open diamond) and KCL22/HA (open square). (b) Light microscopy analysis of K562-HA cells 12 h after treatment with Rakicidin A (0.25 μM). Morphology of untreated healthy K562-HA (left) and apoptotic cells (right) showed shrinkage, nuclear condensation and fragmentation. Original magnification, ×400.

doi: 10.1111/j.1349-7006.2010.01813.x
© 2010 Japanese Cancer Association

Results

Hypoxia adaptation induced TKI resistance in CML cells. To confirm the effect of TKI on hypoxia-adaptation in CML cells,[13] sensitivity to imatinib and dasatinib was investigated in HA-CML cells. The IC_{50} values of imatinib in K562, K562-HA, KCL22 and KCL22-HA cells were 1.36, 41.5, 25.9 and 57.6 μM, respectively. The K562-HA and KCL22-HA cells were highly resistant to imatinib compared to the parental K562 and KCL22 cells, respectively (Fig. 1a). The anti-proliferative effect of dasatinib, which has higher affinity for Abl than imatinib, was also examined in the HA-CML cells and their parental cells. The IC_{50} values of dasatinib for K562 and K562-HA were 0.514 and 2.7 nM, respectively. The IC_{50} values of dasatinib in KCL22 and KCL22-HA cells could not be evaluated. The K562-HA cells were less sensitive than the K562 cells; however, both KCL22-HA and KCL22 cells were less sensitive to dasatinib (Fig. 1b). These results indicated that the K562-HA and KCL22-HA cells were resistant to TKI.

Rakicidin A-induced apoptosis in HA-CML cells. Recently, Yamazaki *et al.*[14] screened 20 000 cultured broths of microorganisms and isolated Rakicidin A, a highly hypoxia-selective cytotoxic compound from *Micromonospora* strain ML99-43F1. The inhibitory effects of Rakicidin A on HA-CML or their parental CML cells was investigated, and the IC_{50} values of Rakicidin A in K562, K562-HA, KCL22 and KCL22-HA cells were 5.24, 1.55, 5.45 and 1.64 μM, respectively. Rakicidin A elicited an approximately fivefold increase in the cytotoxic effects in HA-CML cells compared with the parental cells (Fig. 2a). Examination by light microscopy showed that Rakicidin A treatment induced cell shrinkage, nuclear condensation and fragmentation, which are typical in cells undergoing apoptosis (Fig. 2b). Therefore, Annexin-V staining and mitochondrial outer membrane permeabilization with $DiOC_6$ was used to determine the mechanism of cell death induced by Rakicidin A. The percentage of cells undergoing apoptosis was greater in Rakicidin A-treated K562-HA and KCL22-HA cells than in parental K562 and KCL22 cells (Fig. 3a).

Next, the effects of Rakicidin A on the cell cycle were examined. In both K562-HA and KCL22-HA cells, the number of cells in the subG1 fraction was increased (Fig. 3b), and DNA fragmentation was detected in all phases of the cell cycle in the K562-HA cells (Fig. S1). These findings indicated that Rakicidin A induced apoptotic cell death in HA-CML cells independent of the cell cycle.

Effects of Rakicidin A in normal hematopoietic progenitors and primary CML cells. The effect of Rakicidin A on normal hematopoietic progenitors and primary CML cells was then investigated. When normal progenitor cells were treated with 0.25 μM

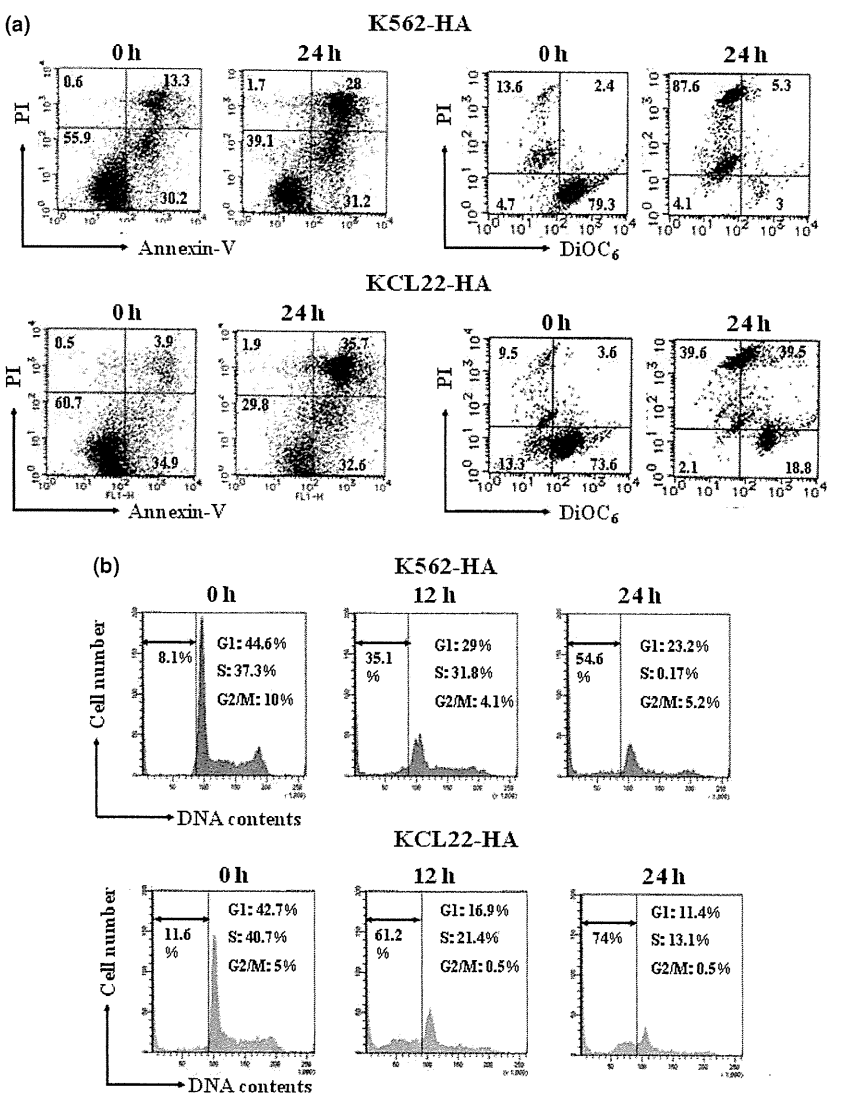

Fig. 3. Induction of apoptosis by Rakicidin A. Flow cytometric analysis of K562-HA (upper panels) and KCL22-HA (lower panels) cells treated with 0.25 μM Rakicidin A for the indicated periods of time. (a) Cells were simultaneously stained with Annexin-V to determine the expression of phosphatidylserine or stained with 3,3′-dihexyloxacarbocyanine iodide ($DiOC_6$) to determine the mitochondrial transmembrane potential, and propidium iodide (PI) to determine the cell viability. (b) Flow cytometric analysis of K562-HA and KCL22-HA cells using PI was performed after 12 and 24 h of Rakicidin A treatment (0.25 μM). The numbers inside each histogram indicate the percentage of the sub G1 fraction. K562-HA (upper panels) and KCL22-HA (lower panels) DNA fragmentation was detected Rakicidin A (0.25 μM) treatment using incorporation of biotinylated nucleotides into the DNA by TdT at the indicated time.

© 2010 Japanese Cancer Association

Rakicidin A at 20% O_2 or 1% O_2, the CFC were 113% ± 8% of the untreated control in 20% O_2 and 36% ± 12% of untreated control in 1% O_2. The CFC of primary CML cells were treated with 0.125 and 0.25 μM Rakicidin A at 20% O_2 or 1% O_2, the CFC were 92% ± 23% of untreated control and 93% ± 21% of untreated control for each Rakicidin A concentrations in 20% O_2, and 45% ± 1% and 6% ± 3% of control in 1% O_2 for each Rakicidin A concentrations in 1% O_2, respectively (Fig. 4). These findings indicated that Rakicidin A selectively inhibited colony formation in cells derived from CML patients under hypoxic conditions.

Activation of caspase-3 by Rakicidin A. To investigate the mechanism of Rakicidin A-induced apoptosis, the effect of Rakicidin A on the $\Delta\psi$m was investigated. In the HA-CML cells, treatment with Rakicidin A decreased the $\Delta\psi$m, suggesting that Rakicidin A activated the mitochondria-mediated apoptosis pathway in these cells. Additionally, fluorometric analysis of caspase activity in the HA-CML cells demonstrated that Rakicidin A activated caspase-3 (Fig. S2). Therefore, we next examined whether inhibiting caspase-3 activity prevented Rakicidin A from inducing cell death in the HA-CML cells. Although caspase-3 activity was effectively blocked by pre-treatment with zVAD (Fig. S2), cell death was still induced, although it was significantly delayed (Fig. 5). These findings suggested that Rakicidin A-induced apoptosis in HA-CML cells is mediated only partially via the mitochondria-mediated pathway and that an alternative mitochondria-independent pathway may exist.

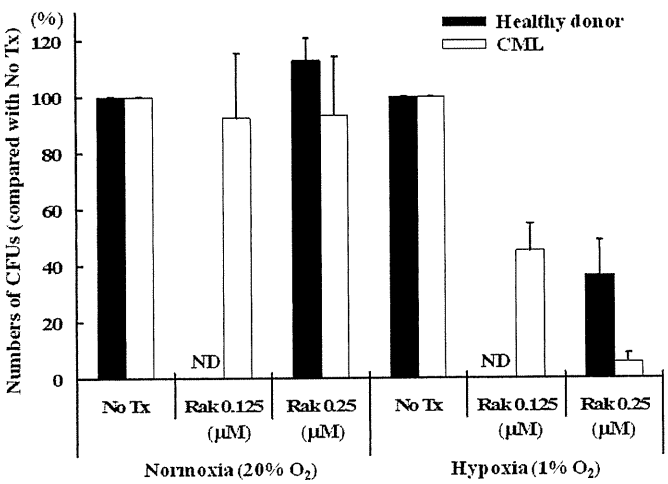

Fig. 4. The effects of Rakicidin A (Rak) in normal hematopoietic progenitors and primary chronic myelogenous leukemia (CML) cells. The effects of Rak on normal hematopoietic progenitors and primary CML cells was investigated using a standard methylcellulose culture assay as described in the Materials and Methods. The rates of inhibitory effects on the colony-forming unit (CFU) in normal progenitor (black bars) and primary CML cells (white bars) at each indicated concentration of Rakicidin A compared with the number of colony-forming cells without Rakicidin A were examined using a colony assay. ND, not done.

Effect of combined treatment with Rakicidin A and imatinib on HA-CML cells. Next, the effect of treatment with both Rakicidin A and imatinib was evaluated in the HA-CML cells. Combination indexes (CI) were calculated according to the method of Chou using CalcuSyn for Windows software as described elsewhere.[15,16,21] This method provides quantitation of synergism (CI <1) and antagonism (CI >1) at different doses and effect levels. The combination of imatinib and Rakicidin A induced a synergistic effect on cell death in both HA-CML cell lines (Fig. 6a–d). In the parental K562 and KCL22 cells, combined treatment is antagonistic rather than synergistic (Fig. 6c–f). These observations suggest that concomitant treatment with Rakicidin A and imatinib selectively augmented growth inhibition of leukemic cells under hypoxic conditions, such as those found in the BM.

Discussion

The prognosis of CML patients has been drastically improved by the use of TKI; however, the success of treatment is still plagued by problems that lead to CML relapse, such as resistance to TKI.[11,22] The TKI are able to kill actively proliferating CML cells, whereas resting CML cells are largely resistant to treatment.[23] The CML stem cells are rare and divide less frequently, and thus exist primarily as quiescent cells. Therefore, CML stem cells are resistant to TKI and represent a reservoir for relapse. It is speculated that leukemic stem cells are kept in a quiescent state in the BM niche microenvironment. Recently, it was revealed that leukemic stem cells that reside within the endosteal region exhibit relatively high resistance to anticancer drugs.[24] In particular, the

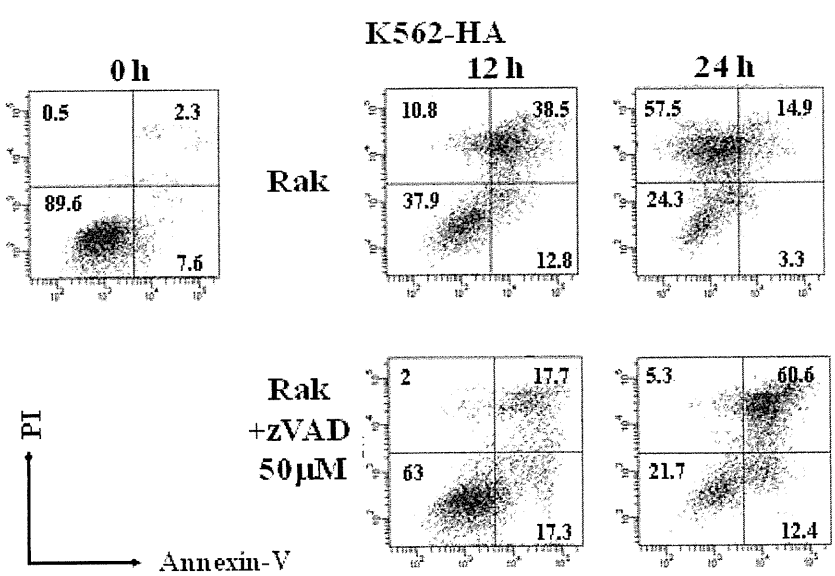

Fig. 5. The Rakicidin A inducing apoptosis delayed effect of pan-caspase inihibitor, zVAD. Effects of pre-treatment with or without 50 μM zVAD on K562-HA cell death induced by 0.25 μM Rakicidin A at the indicated periods. zVAD did not prevent cell death by Rakicidin A treatment, but showed a delay in Rakicidin A-inducing apoptosis (lower panels). PI, propidium iodide.

doi: 10.1111/j.1349-7006.2010.01813.x
© 2010 Japanese Cancer Association

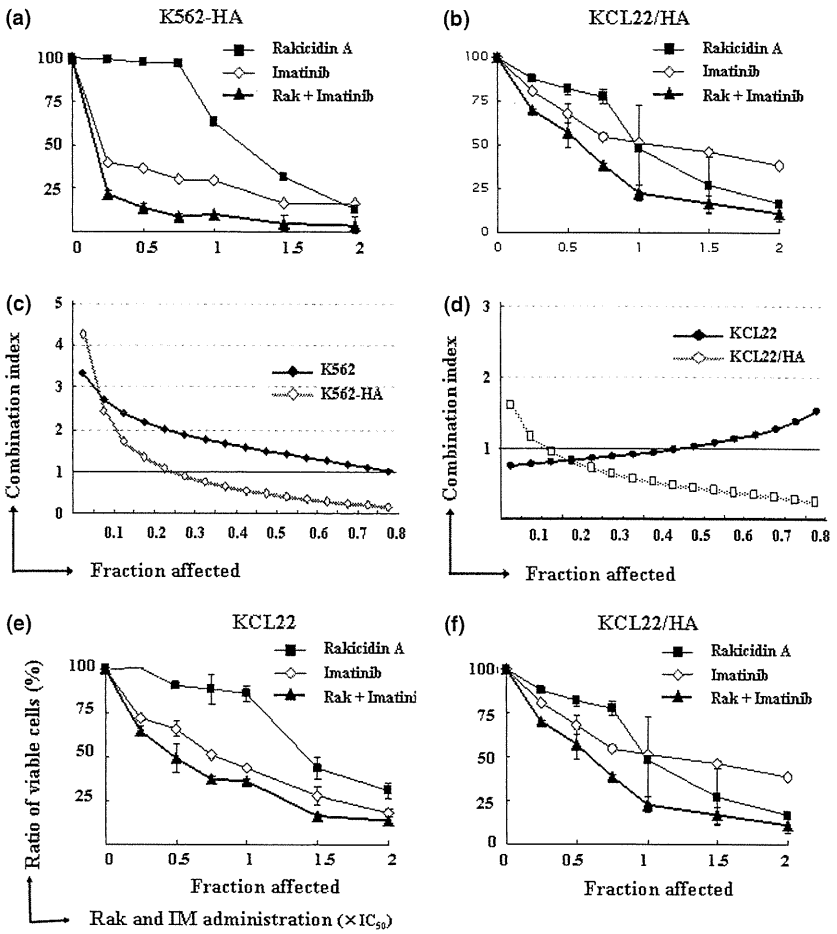

Fig. 6. The combined effects of imatinib amd Rakicidin A on K562 and K562-HA. Evaluation of the combined effects of imatinib and Rakicidin A on K562-HA (a) and KCL22-HA (b). Cells were incubated for 48 h with six concentrations (0.25, 0.5, 0.75, 1, 1.5 or 2 times the IC_{50}) of each agent or both in combination. The IC_{50} of Imatinib and Rakicidin A were previously described in Figure 1(a–c). The killing curves of the concurrent administration of imatinib and Rakicidin A are shown. (c,d) The combination index (CI)-fraction affected (Fa) plots are shown. The combination index was determined with the nonlinear regression program CalcuSyn. The combined effects of imatinib and Rakicidin A on K562 (e) and KCL22 (f) were also evaluated as described above.

BM endosteum is recognized as a severely hypoxic region. Hypoxia maintains both normal and leukemic stem cells in the resting phase.[6,25] Previously, we investigated the microenvironment of leukemic cells in the BM and confirmed that leukemic cells survived under severely hypoxic conditions, resulting in resistance to TKI and other anticancer agents (Fig. 1).[13] Additionally, hypoxia inhibits Bcr-Abl phosphorylation and fosters the establishment of a more primitive population of CML cells, which might explain why those cells are less sensitive to TKI.[13,26,27] Therefore, the development of a novel therapeutic approach for targeting hypoxic cells in the BM may lead to a cure for CML patients.

Although the target molecule of Rakicidin A has not been identified, Rakicidin A exhibits approximately 17.5-fold more cytotoxicity in solid tumor cells in a hypoxic environment compared with cells in normoxic conditions.[14] The cytotoxic effect of Rakicidin A was also observed under transient hypoxic conditions, but Rakicidin A exhibited the highest degree of cytotoxicity in CML cells incubated under long term hypoxic conditions (Fig. 2a). It is believed that CML stem cells reside in the juxta endosteum lesion or niche, which allows the leukemic cells to evade cell-death stimuli.[28,29] Hypoxia is one of the important factors that constitute the BM niche.[30] Thus, the hypoxia-specific cytotoxicity induced by Rakicidin A may be able to eradicate leukemic stem cells.

We demonstrated that Rakicidin A inhibited the proliferation of HA-CML cells by inducing apoptosis. As shown in Figure 4a, Rakicidin A decreased the mitochondrial transmembrane potential in HA-CML cells, indicating that Rakicidin A induces apoptosis through the intrinsic pathway. However, treatment with zVAD, a pan-caspase inhibitor that blocks the activation of caspase-3, delayed but did not prevent apoptosis in K562-HA cells. The delayed apoptotic response was also observed in UV-irradiated Hela cells, due to suppressed caspase-3 activity and reduced activity of the caspases downstream of cytochrome *c* release.[31] These different responses to apoptotic stimuli may depend on cell-type specific apoptosis signalling pathways. It can be speculated that Rakicidin A also activates caspase-independent apoptosis pathways in HA-CML cells, such as apoptosis inducing factor (AIF) or Calpain.[32,33] Further investigation is necessary to clarify this issue.

Novel hypoxia-sensitizers including tirapazamine, a reducing agent, and HIF-1 inhibitor, including gene therapy, have recently been developed.[34–38] Moreover, several anticancer agents inhibit the proliferation of cancer cells by producing reactive oxygen species.[39,40] However, Rakicidin A does not act as a reductant because Rakicidin A has neither nitric oxide (NO) residues nor quinones in its structure. In addition, Rakicidin does not increase the transcriptional activity of HIF-1.[14] Interestingly, a previous study reported that Rakicidin A failed to induce apoptosis in solid cancer cells.[14] Further investigation is required to clarify the cytotoxic mechanisms of Rakicidin A in different cancer cell types.

In conclusion, Rakicidin A effectively induced apoptosis in HA-CML cells with primitive characteristics. Additionally, combined treatment with Rakicidin A and imatinib exhibited synergistic cytotoxic effects in HA-CML cells. These observations suggest that Rakicidin A may be a useful agent for the eradication of CML stem cells.

© 2010 Japanese Cancer Association

Acknowledgments

This work was supported by a Grant-in-Aid for Scientific Research from the Ministry of the Education, Culture, Sports, Science, and Technology of Japan and grants from the Yasuda Medical Foundation and the Fujiwara Memorial Foundation.

Disclosure Statement

The authors have no conflict of interest.

References

1 Vaupel P, Kelleher DK, Hockel M. Oxygenation status of malignant tumors: pathogenesis of hypoxia and significance for tumor therapy. *Semin Oncol* 2001; **28**: 29–35.
2 Kizaka-Kondoh S, Inoue M, Harada H *et al.* Tumor hypoxia: a target for selective cancer therapy. *Cancer Sci* 2003; **94**: 1021–8.
3 Gatenby RA, Gillies RJ. Why do cancers have high aerobic glycolysis? *Nat Rev Cancer* 2004; **4**: 891–9.
4 Brown JM, Wilson WR. Exploiting tumour hypoxia in cancer treatment. *Nat Rev Cancer* 2004; **6**: 437–47.
5 Hockel M, Schlenger K, Aral B *et al.* Association between tumor hypoxia and malignant progression in advanced cancer of the uterine cervix. *Cancer Res* 1996; **56**: 4509–15.
6 Parmar K, Mauch P, Vergilio JA *et al.* Distribution of hematopoietic stem cells in the bone marrow according to regional hypoxia. *Proc Natl Acad Sci U S A* 2007; **104**: 5431–6.
7 Cipolleschi MG, Dello Sbarba P, Olivotto M. The role of hypoxia in the maintenance of hematopoietic stem cells. *Blood* 1993; **82**: 2031–7.
8 Sawyers CL. Chronic myeloid leukemia. *N Engl J Med* 1999; **340**: 1330–40.
9 Goldman JM, Melo JV. Chronic myeloid leukemia-advances in biology and new approaches to treatment. *N Engl J Med* 2003; **349**: 1451–64.
10 Druker BJ, Guilhot F, O'Brien SG *et al.* Five-year follow-up of patients receiving imatinib for chronic myeloid leukemia. *N Engl J Med* 2006; **355**: 2408–17.
11 Michor F, Hughes TP, Iwasa Y *et al.* Dynamics of chronic myeloid leukaemia. *Nature* 2005; **435**: 1267–70.
12 Copland M, Hamilton A, Elrick LJ *et al.* Dasatinib (BMS-354825) targets an earlier progenitor population than imatinib in primary CML but does not eliminate the quiescent fraction. *Blood* 2006; **107**: 4532–9.
13 Takeuchi M, Kimura S, Kuroda J *et al.* Glyoxalase-I is a novel target against Bcr-Abl^{+} leukemic cells acquiring stem-like characteristics in hypoxic environment. *Cell Death Differ* 2010; **17**: 1211–20.
14 Yamazaki Y, Kunimoto S, Ikeda D. Rakicidin A: a hypoxia-selective cytotoxin. *Biol Pharm Bull* 2007; **30**: 261–5.
15 Chou TC. Drug combination studies and their synergy quantification using the Chou–Talay method. *Cancer Res* 2010; **70**: 440–6.
16 Chou TC. Theoretical basis, experimental design, and computerized simulation of synergism and antagonism in drug combination studies. *Pharmacol Rev* 2006; **58**: 621–81.
17 Kimura S, Kuroda J, Segawa H *et al.* Antiproliferative efficacy of the third generation bisphosphate zoledronic acid combined with other anticancer drugs in leukemic cell lines. *Int J Hematol* 2004; **79**: 37–43.
18 Kamitsuji Y, Kuroda J, Kimura S *et al.* Bcr-Abl kinase inhibitor INNO-406 induces autophagy and different modes of cell death execution in Bcr-Abl-positive leukemias. *Cell Death Differ* 2008; **15**: 1712–22.
19 Kimura S, Maekawa T, Hirakawa K *et al.* Alterations of c-myc expression by antisense oligodeoxynucleotides enhance the induction of apoptosis in HL-60 cells. *Cancer Res* 1995; **55**: 1379–84.
20 Okada M, Adachi S, Imai T *et al.* A novel mechanism for imatinib mesylate-induced cell death of BCR-ABL-positive human leukemic cells: caspase-independent, necrosis-like programmed cell death mediated by serine protease activity. *Blood* 2004; **103**: 2299–307.
21 Kawata E, Asihara E, Nakagawa Y *et al.* A combination of a DNA-chimera siRNA against PLK-1 and zoledronic acid supresses the growth of malignant methothelioma cells *in vitro*. *Cancer Lett* 2010; **294**: 245–53.
22 Tanaka R, Kimura S. From the second generation Abl tyrosine kinase inhibitors to the next generation for overriding Bcr-Abl/T315I. *Expert Rev Anticancer Ther* 2008; **8**: 1387–98.
23 Graham SM, Jørgensen HG, Allan E. Primitive, quiescent, Philadelphia-positive stem cells from patients with chronic myeloid leukemia are insensitive to STI571 *in vitro*. *Blood* 2002; **99**: 319–25.
24 Ishikawa F, Yoshida S, Saito Y *et al.* Chemotherapy-resistant human AML stem cells home to engraft within the bone-marrow endosteal region. *Nat Biotechnol* 2007; **25**: 1315–21.
25 Jensen PØ, Mortensen BT, Hodgkiss RJ *et al.* Increased cellular hypoxia and reduced proliferation of both normal and leukaemic cells during progression of acute myeloid leukaemia in rats. *Cell Prolif* 2000; **33**: 381–95.
26 Giuntoli S, Rovida E, Barbetti V. Hypoxia suppresses BCR/Abl and selects imatinib-insensitive progenitors within clonal CML populations. *Leukemia* 2006; **20**: 1291–3.
27 Giuntoli S, Rovida E, Gozzini A. Severe hypoxia defines heterogeneity and selects highly immature progenitors within clonal erythroleukemia cells. *Stem Cells* 2007; **25**: 1119–25.
28 Ninomiya M, Abe A, Katsumi A *et al.* Homing, proliferation and survival sites of human leukemia cells *in vivo* in immunodeficient mice. *Leukemia* 2007; **21**: 136–42.
29 Hochhaus A, La Rosée P. Imatinib therapy in chronic myelogenous leukemia: strategies to avoid and overcome resistance. *Leukemia* 2004; **18**: 1321–31.
30 Desplat V, Faucher JL, Mahon FX *et al.* Hypoxia modifies proliferation and differentiation of CD34(+) CML cells. *Stem Cells* 2002; **20**: 347–54.
31 Sasai K, Yajima H, Suzuki F. Suppression of postmitochondrial signaling and delayed response to UV-induced nuclear apoptosis in HeLa cells. *Jpn J Cancer Res* 2002; **93**: 275–83.
32 Cande C, Cohen I, Daugas E *et al.* Apoptosis-inducing factor (AIF): a novel caspase-independent death effector released from mitochondria. *Biochimie* 2002; **84**: 215–22.
33 Liu L, Xing D, Chen WR. Micro-calpain regulates caspase-dependent and apoptosis inducing factor-mediated caspase-independent apoptotic pathways in cisplatin- induced apoptosis. *Int J Cancer* 2009; **12**: 2757–66.
34 Zeman EM, Brown JM, Lemmon MJ *et al.* SR-4233: a new bioreductive agent with high selective toxicity for hypoxic mammalian cells. *Int J Radiat Oncol Biol Phys* 1986; **12**: 1239–42.
35 Brown JM. The hypoxic cell: a target for selective cancer therapy. *Cancer Res* 1999; **59**: 5863–70.
36 Shibata T, Shibamoto Y, Sasai K *et al.* Comparison of *in vivo* efficacy of hypoxic cytotoxin tirapazamine and hypoxic cell radiosensitizer KU-2285 in combination with single and fractionated irradiation. *Jpn J Cancer Res* 1996; **87**: 98–104.
37 Masunaga S, Ono K, Suzuki M *et al.* Usefulness of tirapazamine as a combined agent in chemoradiation and thermo-chemoradiation therapy at mild temperatures: reference to the effect on intratumor quiescent cells. *Jpn J Cancer Res* 2000; **91**: 566–72.
38 Liu F, Wang P, Jiang X *et al.* Antisense hypoxia-inducible factor 1alpha gene therapy enhances the therapeutic efficacy of doxorubicin to combat hepatocellular carcinoma. *Cancer Sci* 2008; **99**: 2055–61.
39 Doroshow JH. Role of hydrogen peroxide and hydroxyl radical formation in the killing of Ehrlich tumor cells by anticancer quinines. *Proc Natl Acad Sci U S A* 1986; **83**: 4514–18.
40 Shinha BK, Mimnaugh EG. Free radicals and anticancer drug resistance: oxygen free radicals in the mechanisms of drug cytotoxicity and resistance by certain tumors. *Free Radic Biol Med* 1990; **8**: 567–81.

Supporting Information

Additional Supporting Information may be found in the online version of this article:

Fig. S1. Effects of Rakicidin A on K562-HA cells.

Fig. S2. The effects of Caspase-3 activation with or without Rakicidin A and/or zVAD on K562-HA cells.

Please note: Wiley-Blackwell are not responsible for the content or functionality of any supporting materials supplied by the authors. Any queries (other than missing material) should be directed to the corresponding author for the article.

doi: 10.1111/j.1349-7006.2010.01813.x
© 2010 Japanese Cancer Association

Chemistry & Biology
Article

Identification of a Small-Molecule Inhibitor of DNA Topoisomerase II by Proteomic Profiling

Makoto Kawatani,[1] Hiroshi Takayama,[1,2] Makoto Muroi,[1] Shinya Kimura,[3] Taira Maekawa,[4] and Hiroyuki Osada[1,2,*]
[1]Chemical Biology Core Facility, Chemical Biology Department, RIKEN Advanced Science Institute, Saitama 351-0198, Japan
[2]Graduate School of Science and Engineering, Saitama University, Saitama 338-8570, Japan
[3]Department of Internal Medicine, Faculty of Medicine, Saga University, Saga 849-8501, Japan
[4]Department of Transfusion Medicine and Cell Therapy, Kyoto University Hospital, Kyoto 606-8507, Japan
*Correspondence: hisyo@riken.jp
DOI 10.1016/j.chembiol.2011.03.012

SUMMARY

BNS-22, a chemically synthesized derivative of the natural plant product GUT-70, has antiproliferative activity against human cancer cells, the mechanism of which is unknown. Here, we identify a target of BNS-22 by proteomic profiling analysis, which suggests that BNS-22 belongs to the same cluster as ICRF-193, a DNA topoisomerase II (TOP2) catalytic inhibitor. BNS-22 inhibits kinetoplast DNA decatenation that is mediated by human TOP2α and TOP2β in vitro at an IC_{50} of 2.8 and 0.42 μM, respectively. BNS-22 does not affect DNA damage and antagonizes TOP2 poison-mediated DNA damage. Like ICRF-193, BNS-22 induces mitotic abnormalities, characterized by impairments in chromosome alignment and segregation, thereby causing polyploidy in HeLa cells. These results indicate that BNS-22 targets TOP2 and acts as its catalytic inhibitor.

INTRODUCTION

The promising trends of anticancer drug development programs that were initiated in the early postgenomic era have not translated into many clinical benefits. Researchers, however, have learned much about the host- and cancer-related factors that influence the prognosis of patients who are treated with drugs that have well-defined molecular mechanisms of action. To render a therapy more successful, at least one factor must be elucidated—the precise mechanism of action.

Kimura et al. (2005) reported that the natural product GUT-70, isolated from the stem bark of *Calophyllum brasiliense* in Brazil, inhibits leukemic cell growth and induces caspase-mediated apoptosis. These results prompted us to synthesize derivatives of it that have more robust biological activity; of the more than 60 derivatives of GUT-70, the compound BNS-22 fulfilled this criterion. Yet, its molecular target and mechanism of action remained unknown. A gradual and stepwise analysis of a mechanism of action typically is a long-lasting process that is accompanied by significant degree of uncertainty. Therefore, the best and, hopefully, fastest such approach is a proteomic analysis.

Affinity purification of small-molecule binding proteins using tagged probes, such as biotin conjugates and small-molecule affinity matrices, is a commonly used method (Usui et al., 2004; Teruya et al., 2005; Kawatani et al., 2008). Furthermore, various multidimensional phenotypic profiling methods have been reported to predict target proteins and mechanisms of action of bioactive small molecules, including chemosensitivity profiling of human cancer cell lines (Boyd et al., 2001; Yaguchi et al., 2006), cell morphology–based profiling (Perlman et al., 2004; Young et al., 2008), gene expression profiling (Gunther et al., 2003; Lamb et al., 2006), and chemical proteomics approaches (Bantscheff et al., 2007).

Recently, we reported a proteome-based profiling approach to predict targets of bioactive small molecules using two-dimensional fluorescence differential gel electrophoresis (2D-DIGE) (Muroi et al., 2010). This method is based on recording the comprehensive patterns of variation in proteins in HeLa cells that are treated with small molecules. Our analysis revealed that small molecules that share a molecular target, such as Hsp90 inhibitors (geldanamycin and radicicol), V-ATPase inhibitors (bafilomycin A1 and concanamycin A), and actin inhibitors (cytochalasin D and jasplakinolide), can be grouped into the same cluster. Thus, this proteomic approach is a powerful tool that can be used to classify and predict targets of bioactive small molecules.

Here, we identify a target molecule of BNS-22 by proteomic profiling: DNA topoisomerase II (TOP2). TOP2 is an essential nuclear enzyme that regulates DNA topology and many fundamental processes of DNA metabolism (Champoux, 2001; Wang, 2002; Nitiss, 2009a). TOP2 creates a transient double-strand break in one DNA molecule, through which a second dsDNA molecule is transported (Wang, 2002; Nitiss, 2009a). In mammals, there are two TOP2 isoforms, α and β, which share ~70% sequence identity and have nearly identical catalytic properties in vitro (Austin and Marsh, 1998). They have distinct patterns of expression and physiological functions in mammalian cells (Isaacs et al., 1998). TOP2α expression is cell cycle regulated, peaking in G2/M phase, and is essential for all cells. In contrast, TOP2β expression is independent of the cell cycle and occurs in proliferating and differentiated cells. TOP2β is required for proper neural development in mice (Yang et al., 2000) but is dispensable in other cell types. TOP2α has been proposed to function in growth-dependent processes, such as DNA replication and chromosomal segregation, whereas TOP2β appears to regulate transcription (Ju et al., 2006; Nitiss, 2009a).

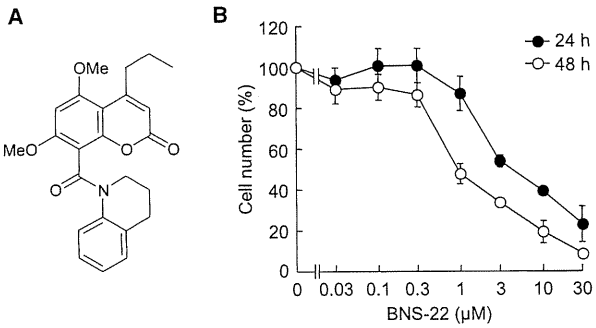

Figure 1. BNS-22 Inhibits the Growth of HeLa Cells
(A) Structure of BNS-22.
(B) Effect of BNS-22 on HeLa cell growth. HeLa cells were treated with the indicated concentrations of BNS-22 for 24 hr and 48 hr. Cell growth was analyzed by WST-8 assay. Cell number (%) indicates the percentage of control. Data are shown as the mean ± SD (n = 3).
See also Figure S1.

In addition to its critical functions, TOP2 is a clinically important target for cancer chemotherapy, and TOP2 inhibitors are vital components in many therapeutic regimens (Nitiss, 2009b; Pommier et al., 2010). TOP2-targeted inhibitors are classified into two groups according to their mechanism of action: TOP2 poisons and catalytic inhibitors. TOP2 poisons, including etoposide (VP-16), daunorubicin, mitoxantrone, and amsacrine, stabilize the reversibly covalent TOP2-DNA complex—termed the cleavable complex—that leads to DNA double-strand break formation, resulting in cancer cell death (Wilstermann and Osheroff, 2003). In contrast, TOP2 catalytic inhibitors block the catalytic center of the enzyme without any association with the formation of cleavable complexes or DNA breaks (Andoh and Ishida, 1998; Larsen et al., 2003). Such agents include ICRF-193 and the structurally related bisdioxopiperazine derivatives (Tanabe et al., 1991), aclarubicin (Jensen et al., 1990), fostriecin, merbarone, suramin, novobiocin, NSC35866 (Jensen et al., 2005), and QAP 1 (Chene et al., 2009). ICRF-193, for example, blocks the intrinsic ATPase activity of TOP2 and traps the enzyme on DNA in its closed clamp form (Roca et al., 1994).

Our data indicate that the TOP2 is the target of BNS-22, as predicted by proteomic profiling, and its mechanism of action entails the inhibition of its catalytic center.

RESULTS

Proteomic Profiling of BNS-22-Treated HeLa Cells

BNS-22 (Figure 1A) inhibited the growth of the human cervix epidermoid carcinoma cell line HeLa in a concentration-dependent manner, as evidenced by the IC_{50} values of 4.9 and 1.0 μM for the 24- and 48-hr treatments, respectively (Figure 1B; see Figure S1 available online). This result indicates that the cytotoxic effects are time dependent, which is typical for enzymatic inhibition rather than instantaneous and temporary cellular damage.

To predict the mechanism of action of BNS-22, we performed proteomic profiling of BNS-22–treated cells by 2D-DIGE. HeLa cells were treated with 10 μM BNS-22 for 18 hr, and the resulting cell lysates were subjected to 2D-DIGE (Figures S2A and S2B). The gel images were linked to our database, which contained images that were generated by 42 well-characterized small molecules. The 296 spots that matched on all gel images were quantified using the 2D-DIGE system software, as described elsewhere (Muroi et al., 2010). Then, hierarchical cluster analysis was performed, and the results were displayed in a heat map and tree diagram. As shown in Figure 2, BNS-22 was clustered with ICRF-193, a TOP2 catalytic inhibitor. In addition, our analysis distinguished between the mechanisms of action of ICRF-193 and etoposide, a TOP2 poison (Figure 2). Our data predict that BNS-22 targets TOP2 and acts as a TOP2 catalytic inhibitor, not a TOP2 poison in cells. Aclarubicin, a known DNA-intercalating agent that prevents the binding of TOP2 to DNA rather than inhibiting its activity, was not clustered with ICRF-193 (Figure 2). This is probably because of the nonspecific effect of aclarubicin, which is known to inhibit other proteins as well, such as TOP1 and the 20S proteasome (Figueiredo-Pereira et al., 1996; Larsen et al., 2003).

BNS-22 Perturbs Mitotic Spindle Formation and Induces Polyploidy

Additional experiments were performed to determine the biological effect of BNS-22 on cell cycle in HeLa cells. By flow cytometry, 24-hr treatment with BNS-22 increased the HeLa cell population in G2/M phase in a concentration-dependent manner (Figure 3A). However, exposure to 3 μM BNS-22 beyond 24 hr was accompanied by the presence of an 8C peak (Figure 3B), characteristic of polyploidal cells. Similar effects were observed in the human promyelocytic leukemia cell line HL-60 (Figure S3).

Thus, we concluded that BNS-22 affects M phase events and disturbs mitotic spindle formation. Moreover, by proteomic profiling, BNS-22 was clustered near typical antimitotic agents, such as vinblastine and nocodazole (Figure 2). To discriminate the effects of these compounds, HeLa cells were exposed to 3 and 10 μM BNS-22, 10 μM ICRF-193, or 300 nM vinblastine for 12 hr and were stained with anti-β-tubulin, anti-γ-tubulin, and DAPI to visualize spindle and chromosomal morphology. ICRF-193 and vinblastine were used as references to differentiate the mechanisms of action. Vehicle-treated control cells and BNS-22-treated cells did not differ morphologically during interphase (Figure 3C), but during mitosis, the control cells harbored a typical bipolar mitotic spindle, whereas BNS-22–treated cells developed abnormal mitotic figures, characterized by unusually distorted spindles and a failure of chromosomal alignment and segregation (Figure 3C). Similar morphological changes were induced by ICRF-193 (Figure S4A), a TOP2 reference compound that was clustered with BNS-22 by proteomic profiling; vinblastine, an antimicrotubular agent, effected dissimilar changes (Figure S4B).

BNS-22 Inhibits TOP2 Activity

To confirm whether BNS-22 inhibits TOP2 enzymatic activity, we measured the effect of BNS-22 on TOP2-mediated kinetoplast DNA decatenation. Kinetoplast DNA is a massive network that consists of thousands of interlocked circular DNA molecules. Because a transient double-strand break is necessary to release circular DNA from the network, the decatenation of kinetoplast

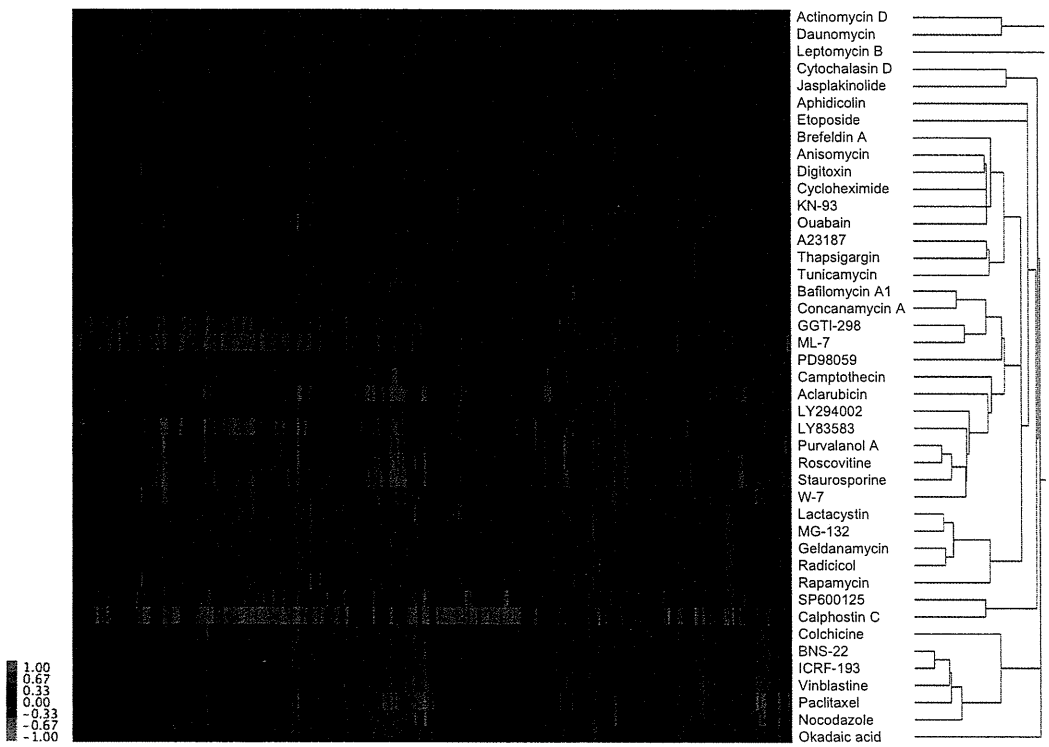

Figure 2. Clustering of BNS-22 and 42 Well-Characterized Compounds by Proteomic Analysis of HeLa Cells

HeLa cells were treated with 10 μM BNS-22 for 18 hr. Proteome analysis was performed using 2D-DIGE. Quantitative data of the 296 spots were combined with data on the 42 well-characterized compounds, and hierarchical clustering was performed. In the heat map, log-fold (natural base) of the normalized volume is shown on the colored scale.

See also Figure S2 and Table S1.

DNA is believed to be a highly specific assay for TOP2 that catalyzes double-strand passing. BNS-22, like ICRF-193, inhibited kinetoplast DNA decatenation by human TOP2α and TOP2β (Figures 4A and 4B). The mean IC_{50} value of BNS-22 for TOP2α and TOP2β, obtained from three independent experiments, was 2.8 ± 1.3 and 0.42 ± 0.09 μM, respectively, as determined by densitometric analysis.

We also observed the effect of BNS-22 on human DNA topoisomerase I (TOP1), which catalyzes topological changes in DNA by transiently introducing single-strand breaks, to determine the selectivity of BNS-22. A TOP1 inhibitor, camptothecin (100 μM), which was used as a positive control, significantly inhibited TOP1 activity, as measured by enzyme-mediated supercoiled DNA relaxation, whereas BNS-22 had no effect at concentrations up to 100 μM (Figure 4C).

BNS-22 Does Not Induce DNA Damage Associated with DNA Double-Strand Breaks

TOP2 inhibitors are classified according to their ability to induce DNA double-strand breaks due to the formation of cleavable complexes (TOP2 poisons) or not (TOP2 catalytic inhibitors), reflecting distinct mechanisms of inhibition. Moreover, TOP2 catalytic inhibitors antagonize TOP2 poison-mediated DNA damage (Ishida et al., 1991; Tanabe et al., 1991). Our proteomic profiling analysis suggested that BNS-22 acts as a TOP2 catalytic inhibitor but not as a TOP2 poison (Figure 2). To confirm this mode of inhibition, we examined the ability of BNS-22 to induce DNA damage, as measured by histone H2AX phosphorylation on serine 139, termed γ-H2AX, a hallmark of DNA double-strand breaks in cells (Rogakou et al., 1998). HeLa cells were treated with 10 μM BNS-22, ICRF-193, or etoposide for 1 hr and were stained with anti-γ-H2AX. Etoposide induced the robust formation of γ-H2AX foci, in contrast to BNS-22 and ICRF-193 (Figure 5A). To determine the antagonistic effects of BNS-22 on etoposide-mediated DNA damage, HeLa cells were pretreated with 10 μM BNS-22 or ICRF-193 for 30 min and were treated with 10 or 30 μM etoposide for 1 hr. By western blot, pretreatment with BNS-22 or ICRF-193 blocked etoposide-induced γ-H2AX accumulation (Figure 5B), suggesting that BNS-22 antagonizes TOP2 poison-mediated DNA damage.

TOP2β is preferentially degraded by the proteasome pathway after cells are exposed to TOP2 poisons or catalytic inhibitors (Mao et al., 2001; Xiao et al., 2003). We recapitulated these effects in HeLa cells that were treated with BNS-22 or ICRF-193; total cellular TOP2β levels declined markedly in a time- and concentration-dependent manner, but TOP2α levels were not significantly affected (Figures 5C and 5D). Considering the predicted mode of action by proteomic profiling and these results, we conclude that BNS-22 functions as a TOP2 catalytic inhibitor.

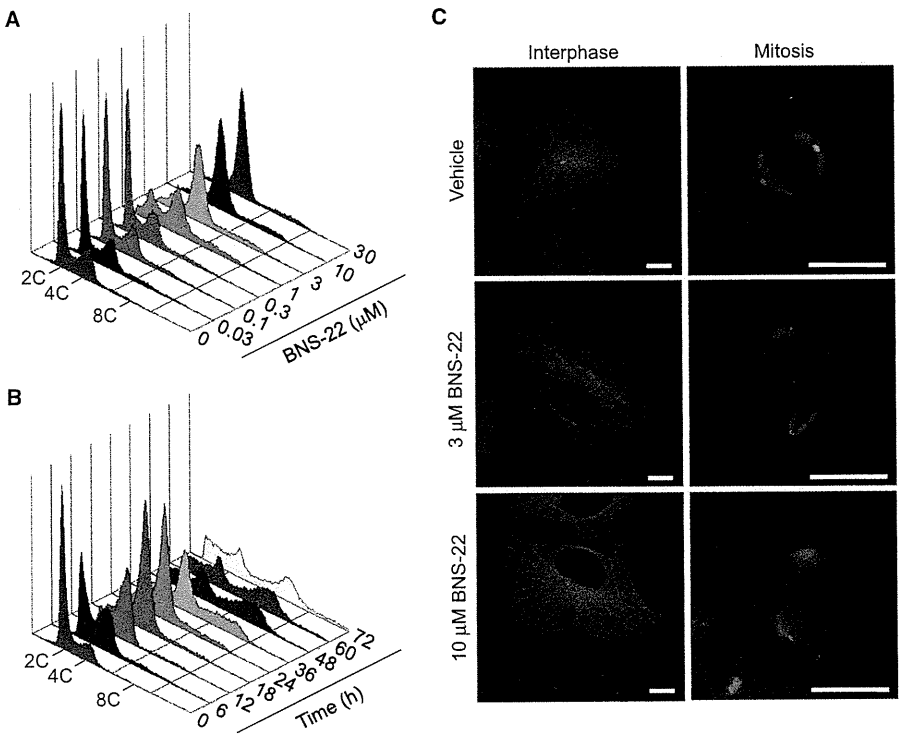

Figure 3. BNS-22 Leads to Mitotic Perturbations

(A and B) Effect of BNS-22 on cell cycle. HeLa cells were treated with the indicated concentrations of BNS-22 for 24 hr (A) or with 3 μM BNS-22 for the indicated times (B). Cells were fixed and analyzed by flow cytometry after propidium iodide staining.

(C) Effect of BNS-22 on mitotic spindle formation. HeLa cells were treated with 3 or 10 μM BNS-22 for 12 hr, fixed, and stained with anti-β-tubulin (green), anti-γ-tubulin (red), and DAPI (blue). Scale bar, 10 μm.

See also Figures S3 and S4.

To examine whether BNS-22 could bind directly to TOP2, we performed affinity precipitation assay using BNS-22–immobilized beads. Purified human TOP2α coprecipitated with BNS-22 beads, and competition was clearly observed in the presence of BNS-22 but was absent with the addition of ICRF-193 (Figure 5E). This result suggests that BNS-22 binds directly to TOP2α in a different mode from ICRF-193.

Structure-Activity Relationship of BNS-22

Structural analogs of BNS-22 were synthesized and tested for their ability to inhibit TOP2 activity (Table 1 and Figure S5). All amides of the N-heterocyclic compound—BNS-51, BNS-52, BNS-53, and BNS-54—failed to inhibit kinetoplast DNA decatenation by human TOP2α at concentrations up to 100 μM. The inhibitory activity BNS-65, an ester of BNS-22, was 3-fold lower than that of BNS-22. These results suggest that the 1,2,3,4-tetrahydroquinoline structure of BNS-22 is essential for the inhibition of TOP2 catalytic activity.

DISCUSSION

A new compound, BNS-22, was determined to possess significant antiproliferative activity against several human cancer cell lines, but its mode of action was unknown. To this end, by proteomic profiling, we found that BNS-22 targets TOP2; in contrast, its mother compound, GUT-70, a natural plant product that has antileukemic activity (Kimura et al., 2005), does not inhibit the DNA decatenation that is mediated by human TOP2α up to 100 μM (Figure S5), indicating that GUT-70 and BNS-22, despite having similar structures, have disparate molecular targets.

Agents that target TOP2 are divided into two classes: TOP2 poisons, which stabilize DNA cleavable complexes and induce DNA damage, and catalytic inhibitors, which interfere with various steps in the catalytic cycle and inhibit growth by abolishing the essential enzymatic activity of TOP2 (Larsen et al., 2003; Wilstermann and Osheroff, 2003). Bisdioxopiperazines, including ICRF-193, are believed to be specific TOP2 catalytic inhibitors, in contrast to most other compounds that are claimed to be catalytic inhibitors of TOP2. BNS-22 induces several cellular phenotypes that are characteristic of bisdioxopiperazines in cells: First, BNS-22 does not induce DNA damage, as evidenced by the lack of γ-H2AX accumulation (Figure 5A), and abrogates TOP2 poison-induced DNA damage (Figure 5B). Second, BNS-22 preferentially degrades TOP2β; TOP2α is unaffected (Figures 5C and 5D). Third, BNS-22 induces mitotic abnormalities that are characterized by the inability of chromosomes to condense and segregate (Figure 3C; Figure S4A),

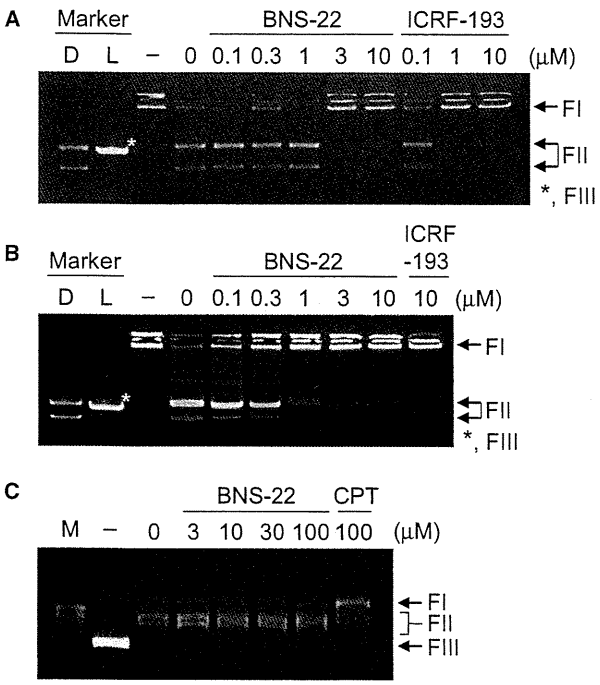

Figure 4. BNS-22 Inhibits TOP2 Activity

(A and B) BNS-22 inhibits human TOP2-mediated kinetoplast DNA decatenation. Catenated kinetoplast DNA was incubated with human TOP2α (A) or TOP2β (B) in the presence of the indicated compounds at 37°C for 30 min. DNA samples were separated by electrophoresis on a 1% agarose gel. The positions of the catenated DNA (FI), decatenated products (FII), and linear DNA (FIII) are indicated. Marker D, decatenated kinetoplast DNA; marker L, linearized kinetoplast DNA; –, no human TOP2α (A) or TOP2β (B).

(C) BNS-22 does not inhibit human TOP1-mediated supercoiled DNA relaxation. Supercoiled plasmid DNA was incubated with human TOP1 in the presence of the indicated compounds at 37°C for 30 min. DNA samples were separated by electrophoresis on a 1% agarose gel. The positions of nicked open circular DNA (FI), relaxed DNA (FII), and supercoiled DNA (FIII) are indicated. M, relaxed plasmid DNA marker; –, no human TOP1; CPT, camptothecin.

resulting in polyploidy (Figure 3B) (Muroi et al., 2010). Thus, these findings strongly suggest that BNS-22 acts as a TOP2 catalytic inhibitor in cells. Several reports suggest that bisdioxopiperazines can induce DNA damage in vitro, both in cell-free and in intact cells, although this remains controversial (Huang et al., 2001; Hajji et al., 2003; Jensen et al., 2004). The results of our study clearly show that ICRF-193 and BNS-22 do not induce DNA damage, thus contrasting the effects of the classical TOP2 poison etoposide on cells (Figures 5A and 5B); therefore, further studies are needed to evaluate the DNA-damaging activity of BNS-22 and ICRF-193 under various experimental conditions.

The inhibitory effects of BNS-22 against TOP2 are well documented, but several compounds possess dual modes of action that allow them to inhibit both TOP1 and TOP2, such as the acridine DACA, the benzopyridoindole intoplicine, the indenoquinolinone TAS-103, the camptothecin analog BN 80927, and the polysaccharide GA3P (Denny and Baguley, 2003; Umemura et al., 2003). TOP1-mediated supercoiled DNA relaxation was not inhibited by BNS-22 at concentrations up to 100 μM (Figure 4C); thus, this new compound must be classified as a specific TOP2 inhibitor, acting by blocking catalytic activity.

The catalytic cycle of TOP2 can be parsed into six discrete steps (Berger et al., 1996; Bates and Maxwell, 2007): (1) binding of TOP2 to DNA, (2) double-stranded cleavage of the DNA, (3) ATP-dependent DNA strand passage, (4) religation of the cleaved DNA, (5) ATP hydrolysis, and (6) enzyme recycling. Agents that inhibit TOP2 act through several mechanisms. For example, aclarubicin blocks enzyme-DNA binding, the initial step of the cycle (Sorensen et al., 1992), and merbarone blocks DNA cleavage (Fortune and Osheroff, 1998). Bisdioxopiperazines inhibit the catalytic cycle of TOP2 by binding near the ATP binding site and trapping the enzyme as a closed clamp on DNA (Classen et al., 2003). Because the interaction between TOP2α and BNS-22 was not inhibited by ICRF-193 (Figure 5E), BNS-22 may bind directly to TOP2 and inhibit its catalytic activity differently from bisdioxopiperazines and, as a consequence, may prevent TOP2 poison-induced DNA damage by stabilizing TOP2-DNA complexes (Figure 5B). However, further investigation is needed to determine the precise mechanism by which BNS-22 inhibits the catalytic activity of TOP2.

The identification of a mode of action is a crucial step during drug development and is important in early preclinical studies, when a substance is transferred from the in vitro to in vivo evaluation stage. The lack of such knowledge can generate disappointing results if a selected cancer does not express a molecular target for an otherwise active compound. Under such circumstances, a compound is judged to be inactive, and in general, further evaluation is halted. Mindful of the possibility for misjudgment, we developed a global system of classifying chemical entities according to their presumably chief mechanism of action, allowing us to make an informed selection of the proper object of evaluation—a tumor. This system allowed us to identify the probable mechanism of action of BNS-22 rapidly, which was confirmed in several steps. Our analysis revealed that small molecules that share a target can be classified by proteomics-based profiling (Muroi et al., 2010). With regard to BNS-22, our cluster analysis distinguished between the mode of action of ICRF-193 and etoposide, although they target the same molecule, TOP2. Our data on BNS-22 demonstrate the effectiveness of target prediction of small molecules by proteomics-based profiling. At this stage, our tool does not need to identify each spot, a generally time-consuming process in proteomic analysis. Nevertheless, characterization of the spots that are altered by treatment with small molecules might increase our understanding of biological pathways and their responses to small molecules. Expansion of the system, by increasing the number of small molecules in the database and identifying spots, will transform it into a more powerful and universal platform, not only to identify mechanisms but also to demonstrate the proof of concept of drugs that enter the clinical phase of evaluation.

TOP2 is an effective target against a wide range of malignancies, and TOP2 poisons, such as etoposide, doxorubicin, and mitoxantrone, have substantial clinical activity. Toxic side effects, however, including drug-induced secondary malignancies, have become a concern in TOP2 poison-based chemotherapy. TOP2 catalytic inhibitors have not been explored extensively

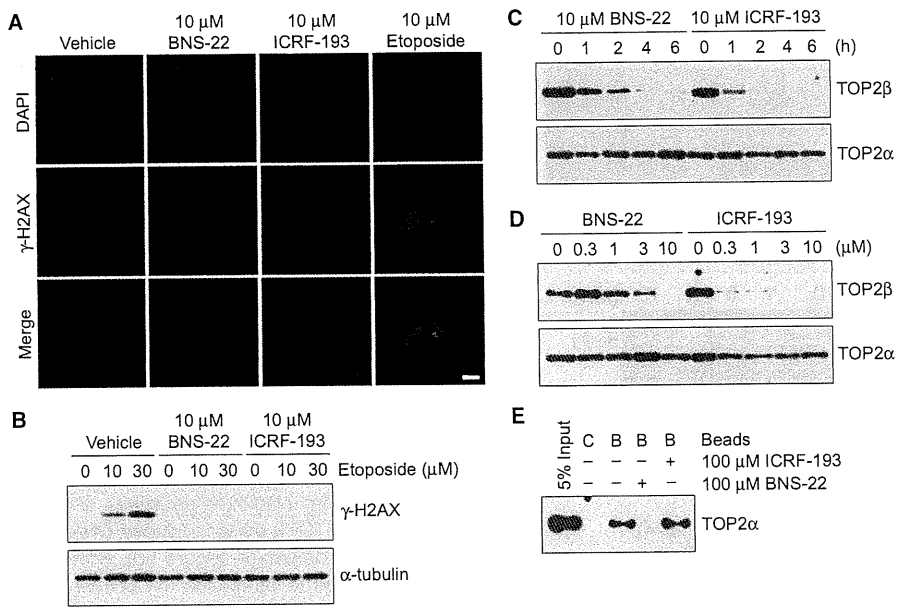

Figure 5. Assessment of Relative Potency of TOP2 Catalytic Inhibitor

(A) BNS-22 does not induce DNA damage. HeLa cells were treated with 10 μM BNS-22, ICRF-193, or etoposide for 1 hr, fixed, and stained with anti-γ-H2AX (green) and DAPI (blue). Scale bar, 10 μm.

(B) BNS-22 antagonizes etoposide-induced DNA damage. HeLa cells were pretreated with 10 μM BNS-22 or ICRF-193 for 30 min and were treated with the indicated concentrations of etoposide for 1 hr. Cell lysates were immunoblotted with anti-γ-H2AX (*top*) and anti-α-tubulin (*bottom*).

(C and D) BNS-22 decreases TOP2β levels. HeLa cells were treated with 10 μM BNS-22 or ICRF-193 for the indicated times (C) or with the indicated concentrations of BNS-22 or ICRF-193 for 6 hr (D). Cell lysates were immunoblotted with anti-TOP2β (*top*) and anti-TOP2α (*bottom*).

(E) BNS-22 binds directly to TOP2α in a different mode than ICRF-193. Purified human TOP2α was incubated with control or BNS-22 beads in the presence or absence of 100 μM BNS-22 or ICRF-193. The reactant beads were washed, and the eluted protein was immunoblotted with anti-TOP2α. C, control beads; B, BNS-22 beads.

in the clinical setting. For instance, bisdioxopiperazines were developed originally as anticancer agents but have been used principally as cardioprotecting agents in the clinic (Larsen et al., 2003). ICRF-187 has clearly been shown to prevent cardiotoxicity that is induced by doxorubicin and other anthracyclines; its ring-opened hydrolysis product is claimed to act as a strong iron chelator, diminishing the harmful effects of reactive oxygen species on heart tissue. The clinical use as anticancer agents is limited to MST-16 (Sobuzoxane), which is a prodrug of ICRF-154. It is active against hematological malignancies but has limited activity toward solid tumors (Larsen et al., 2003).

By definition, TOP2 poison-induced DNA damage can trigger many DNA repair mechanisms; cells that initiate high levels of such activity will resist these cytotoxic effects. Therefore, cancers that lack this capacity are good targets for this treatment. Conversely, TOP2 catalytic inhibitors that do not cause DNA damage should be appropriate candidates for treating cancers with fully active DNA repair systems, which mediate clinical resistance to many anticancer agents. In addition, it is unclear whether resistance to TOP2 poisons is associated with the action of TOP2 catalytic inhibitors (Larsen and Skladanowski, 1998; Larsen et al., 2003). The clinical application of TOP2 catalytic inhibitors has expanded dramatically, according to reports of the involvement of cancer-protective mechanisms in instances of clinical failure. Thus, TOP2 catalytic inhibitors might constitute a second-line treatment in patients who no longer respond to TOP2 poisons, cisplatin, and other agents.

In conclusion, we have demonstrated that BNS-22 targets TOP2 and acts as its catalytic inhibitor in cells. Furthermore, our study shows that proteomics-based profiling will aid in the identification of mechanisms of action of bioactive small molecules in future drug development and chemical genetic studies. Although additional studies are needed, particularly with regard to the molecular mechanism of inhibition by BNS-22 in the catalytic cycle of TOP2 and its in vivo antitumor efficacy, BNS-22 can be used to understand the biochemical and biological functions of TOP2 and administered as an anticancer drug in chemotherapy.

SIGNIFICANCE

Identifying the molecular target of uncharacterized bioactive small molecules is a crucial step in drug development and chemical genetic studies. Recent advances in omics studies and multidimensional analyses have allowed us to profile the effects of drugs by transcript analysis, proteomics, cell phenotype assays, and chemosensitivity. In this study, we identified the target of a small molecule, BNS-22, which has antiproliferative activity against human cancer cells, using our recently developed proteomic profiling

Table 1. In vitro inhibition of TOP2 activity by BNS-22 derivatives

Compound	BNS-22	BNS-51	BNS-52	BNS-53	BNS-54	BNS-65
Structure	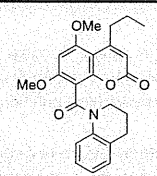	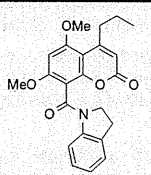	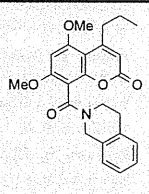	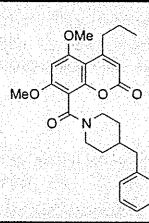	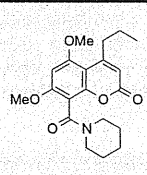	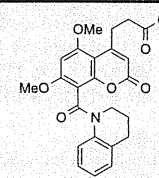
IC_{50} (μM)	2.8	>100	>100	>100	>100	8.2

Catenated kinetoplast DNA was incubated with human TOP2α in the presence of the indicated compounds at 37°C for 30 min. DNA samples were separated by electrophoresis on a 1% agarose gel. The IC_{50} value was determined by densitometric analysis. See also Figures S1 and S5.

approach. We show that BNS-22 targets TOP2 and acts as a catalytic inhibitor in a cell system. TOP2, an essential enzyme that regulates DNA topology, is a clinically important target for cancer chemotherapy. Although various TOP2 poisons, such as etoposide, have been used clinically, the catalytic inhibition of TOP2 has not been explored extensively in cancer treatment. Our study designates a structural class of TOP2 inhibitors that can be used to treat cancers that undergo high levels of DNA repair, compromising the therapeutic effects of DNA-damaging agents.

EXPERIMENTAL PROCEDURES

Materials

The following materials were used: ICRF-193 (Funakoshi); camptothecin (Calbiochem); etoposide, DAPI, anti-α-tubulin, anti-β-tubulin, and anti-γ-tubulin (Sigma-Aldrich); Alexa 488 donkey anti-mouse IgG and Alexa 568 goat anti-rabbit IgG (Molecular Probes); anti-TOP2α (MBL); anti-TOP2β (Santa Cruz Biotechnology); anti-phospho histone H2AX (Ser139) (Upstate); purified human TOP1 (Topogen), purified human TOP2α (Topogen or LAE Biotech International); and purified human TOP2β (LAE Biotech International). The synthesis of BNS-22 and its derivatives is described in Supplemental Experimental Procedures and Figure S1. All compounds were dissolved in dimethylsulfoxide (DMSO) as stock solutions, which were stored at −20°C.

Cell Culture and Cell Growth Assay

The human cervix epidermoid carcinoma cell line HeLa (RIKEN Cell Bank) was cultured in D-MEM (Invitrogen), supplemented with 10% fetal calf serum (Invitrogen), 50 unit/ml penicillin (Invitrogen), and 50 μg/ml streptomycin (Invitrogen), at 37°C in a humidified atmosphere containing 5% CO_2. HeLa cells were seeded in a 96-well culture plate, cultured overnight, and exposed to BNS-22 for the indicated times. After treatment, cell growth was measured using Cell Count Reagent SF (Nacalai Tesque) according to the manufacturer's instruction. Briefly, 1/100 volume of the WST-8 solution was added to each well, and the plates were incubated at 37°C for 1 hr. Then, cell growth was measured as the absorbance at 450 nm on a microplate reader (Perkin Elmer).

Proteome Analysis by 2D-DIGE

Proteome analysis by 2D-DIGE was performed as described elsewhere (Muroi et al., 2010). Briefly, HeLa cells were treated with the designated concentrations of BNS-22 or other inhibitors (Table S1) for 18 hr. Proteome analysis of cell lysates was performed using a 2D-DIGE system (GE Healthcare), and images of the gels were analyzed using Progenesis SameSpots (Nonlinear Dynamics). Of the 298 spots that were described in a previous report, 296 spots were detectable in all gels (Muroi et al., 2010). The volume of each spot was normalized using the average of the corresponding control values from DMSO-treated HeLa cells, and hierarchical clustering analysis was performed.

Flow Cytometric Analysis

HeLa cells were seeded in a 6-well plate and exposed to BNS-22 for the indicated times and concentrations. Cells were harvested, washed with PBS, and fixed in 70% ethanol. Cells were washed twice with PBS again and incubated with 50 μg/ml propidium iodide (Sigma-Aldrich) in PBS containing 2 μg/ml RNase A (Nacalai Tesque) in the dark for 30 min. The DNA content of the cells was analyzed on a Cytomics FC500 (Beckman Coulter).

Immunofluorescence Cell Staining

For β-tubulin and γ-tubulin costaining, cells were cultured on glass coverslips, fixed in methanol for 5 min, and washed with PBS. After blocking with 0.5% BSA in PBS for 5 min at room temperature, the slides were incubated sequentially with primary antibodies, each diluted 1:200 in PBS with 0.5% BSA, for 1 hr at 37°C and with Alexa-conjugated secondary antibodies, each diluted 1:500 in PBS with 0.5% BSA, for 45 min at 37°C.

For phospho-histone H2AX (Ser139) staining, cells that were cultured on glass coverslips were fixed in 3.7% formaldehyde for 20 min, washed with PBS, and permeabilized in 0.2% Triton X-100 in PBS for 5 min at room temperature. After blocking with 0.5% BSA in PBS for 5 min at room temperature, the slides were incubated sequentially with the primary antibody, diluted 1:200 in PBS with 0.5% BSA, for 1 hr at 37°C and with Alexa-conjugated secondary antibody, diluted 1:500 in PBS with 0.5% BSA, for 45 min at 37°C. DNA was stained with 0.1 μg/ml DAPI in PBS. Images were analyzed on a fluorescence microscope (PROVIS AX70, Olympus).

Kinetoplast DNA Decatenation Assay

TOP2 catalytic activity was measured, on the basis of ATP-dependent decatenation of kinetoplast DNA, using the TOP2 assay kit (Topogen). The reaction buffer, containing 50 mM Tris-HCl (pH 8.0), 150 mM NaCl, 10 mM $MgCl_2$, 2 mM ATP, 0.5 mM DTT, and 30 μg/ml BSA for TOP2α, or 40 mM Tris-HCl (pH 7.5), 100 mM KCl, 10 mM $MgCl_2$, 2 mM ATP, 10 mM DTT, 0.5 mM EDTA, and 30 μg/ml BSA for TOP2β, was mixed with 0.2 μg kinetoplast DNA, 1 unit of human TOP2α or TOP2β, and the indicated concentrations of the compounds in a total volume of 20 μl. After incubation at 37°C for 30 min, the reaction was terminated with the addition of 4 μl stop solution. The reaction mixtures were treated with 50 μg/ml proteinase K (Nacalai Tesque) for 30 min at 37°C to digest the protein. Samples were resolved by electrophoresis on a 1% agarose gel containing 0.5 μg/ml ethidium bromide in TAE buffer. DNA bands were visualized by UV exposure and photographed on a UV transilluminator. Fluorescent bands were quantitated by scanning the agarose gels on a Typhoon 9400 Variable Mode Imager (GE Healthcare).

Supercoiled DNA Relaxation Assay

TOP1 activity was measured, on the basis of the relaxation of supercoiled DNA, using the TOP1 assay kit (Topogen). DNA relaxation assay was performed according to the manufacturer's instruction. Reaction buffer, containing 10 mM Tris-HCl (pH 7.9), 150 mM NaCl, 1 mM EDTA, 0.1% BSA, 0.1 mM spermidine, and 5% glycerol, was mixed with 0.25 μg of supercoiled DNA, 4 units of human TOP1, and the indicated concentrations of the compounds in a total volume of 20 μl. After incubation at 37°C for 30 min, the reaction

was terminated with the addition of 2 μl 10% SDS. The reaction mixtures were treated with 50 μg/ml proteinase K for 30 min at 37°C to digest the protein. Two microliters of loading buffer was added, and the DNA was extracted once with CIA (chloroform:isoamyl alcohol, 24:1). Samples were resolved by electrophoresis on a 1% agarose gel, after which the gel was stained with 0.5 μg/ml ethidium bromide in TAE buffer for 30 min. DNA bands were visualized by UV exposure and photographed on a UV transilluminator.

Western Blot

Western blot was performed as described with slight modifications (Woo et al., 2006). Briefly, cell lysates were prepared in RIPA buffer (25 mM HEPES [pH 7.8], 0.5 M NaCl, 5 mM EDTA, 1.5% Triton X-100, 1.0% sodium deoxycholate, 0.1% SDS, and 5 mM EDTA), supplemented with a protease inhibitor cocktail (Roche). Samples were subjected to SDS-PAGE and transferred to a PVDF membrane (Immobilon P, Millipore). Membranes were incubated with the indicated primary antibodies and horseradish peroxidase–labeled secondary antibodies and visualized by exposure to X-ray film using SuperSignal West Pico Chemiluminescence Substrate (Pierce).

BNS-22 Binding Assay

BNS-22–immobilized beads were prepared as described elsewhere (Kanoh et al., 2005; Kawatani et al., 2008). Purified human TOP2α (500 ng) was incubated with control or BNS-22 beads (20 μl) in the presence or absence of 100 μM BNS-22 or 100 μM ICRF-193 in binding buffer containing 40 mM Tris-HCl (pH 7.5), 100 mM KCl, 10 mM $MgCl_2$, 0.5 mM EDTA, 5 mM DTT, 2 mM ATP, and 0.1% BSA in a total volume of 1 ml for 3 hr at 4°C. The reactant beads were washed with binding buffer without BSA, and the bound protein was eluted with SDS-PAGE sample buffer. The sample was resolved by SDS-PAGE and detected by western blot with anti-TOP2α.

SUPPLEMENTAL INFORMATION

Supplemental Information includes five figures, one table, and Supplemental Experimental Procedures and can be found with this article online at doi:10.1016/j.chembiol.2011.03.012.

ACKNOWLEDGMENTS

We thank Nippon Shinyaku Co., Ltd. for providing the compounds, H. Kondo and K. Noda for the proteome analysis, S. Kazami and K. Tomita for cell staining, H. Aono for cell culture, and K. Wierzba and T. Shimizu for critically reading the manuscript. This work was supported in part by a Grant-in-Aid from the Ministry of Education, Culture, Sports, Science, and Technology of Japan. The authors declare no competing financial interests.

Received: November 1, 2010
Revised: March 29, 2011
Accepted: March 30, 2011
Published: June 23, 2011

REFERENCES

Andoh, T., and Ishida, R. (1998). Catalytic inhibitors of DNA topoisomerase II. Biochim. Biophys. Acta *1400*, 155–171.

Austin, C.A., and Marsh, K.L. (1998). Eukaryotic DNA topoisomerase IIβ. Bioessays *20*, 215–226.

Bantscheff, M., Eberhard, D., Abraham, Y., Bastuck, S., Boesche, M., Hobson, S., Mathieson, T., Perrin, J., Raida, M., Rau, C., et al. (2007). Quantitative chemical proteomics reveals mechanisms of action of clinical ABL kinase inhibitors. Nat. Biotechnol. *25*, 1035–1044.

Bates, A.D., and Maxwell, A. (2007). Energy coupling in type II topoisomerases: why do they hydrolyze ATP? Biochemistry *46*, 7929–7941.

Berger, J.M., Gamblin, S.J., Harrison, S.C., and Wang, J.C. (1996). Structure and mechanism of DNA topoisomerase II. Nature *379*, 225–232.

Boyd, M.R., Farina, C., Belfiore, P., Gagliardi, S., Kim, J.W., Hayakawa, Y., Beutler, J.A., McKee, T.C., Bowman, B.J., and Bowman, E.J. (2001). Discovery of a novel antitumor benzolactone enamide class that selectively inhibits mammalian vacuolar-type (H^+)-ATPases. J. Pharmacol. Exp. Ther. *297*, 114–120.

Champoux, J.J. (2001). DNA topoisomerases: structure, function, and mechanism. Annu. Rev. Biochem. *70*, 369–413.

Chene, P., Rudloff, J., Schoepfer, J., Furet, P., Meier, P., Qian, Z., Schlaeppi, J.M., Schmitz, R., and Radimerski, T. (2009). Catalytic inhibition of topoisomerase II by a novel rationally designed ATP-competitive purine analogue. BMC Chem. Biol. *9*, 1.

Classen, S., Olland, S., and Berger, J.M. (2003). Structure of the topoisomerase II ATPase region and its mechanism of inhibition by the chemotherapeutic agent ICRF-187. Proc. Natl. Acad. Sci. USA *100*, 10629–10634.

Denny, W.A., and Baguley, B.C. (2003). Dual topoisomerase I/II inhibitors in cancer therapy. Curr. Top. Med. Chem. *3*, 339–353.

Figueiredo-Pereira, M.E., Chen, W.E., Li, J., and Johdo, O. (1996). The antitumor drug aclacinomycin A, which inhibits the degradation of ubiquitinated proteins, shows selectivity for the chymotrypsin-like activity of the bovine pituitary 20 S proteasome. J. Biol. Chem. *271*, 16455–16459.

Fortune, J.M., and Osheroff, N. (1998). Merbarone inhibits the catalytic activity of human topoisomerase IIα by blocking DNA cleavage. J. Biol. Chem. *273*, 17643–17650.

Gunther, E.C., Stone, D.J., Gerwien, R.W., Bento, P., and Heyes, M.P. (2003). Prediction of clinical drug efficacy by classification of drug-induced genomic expression profiles *in vitro*. Proc. Natl. Acad. Sci. USA *100*, 9608–9613.

Hajji, N., Pastor, N., Mateos, S., Dominguez, I., and Cortes, F. (2003). DNA strand breaks induced by the anti-topoisomerase II bis-dioxopiperazine ICRF-193. Mutat. Res. *530*, 35–46.

Huang, K.C., Gao, H., Yamasaki, E.F., Grabowski, D.R., Liu, S., Shen, L.L., Chan, K.K., Ganapathi, R., and Snapka, R.M. (2001). Topoisomerase II poisoning by ICRF-193. J. Biol. Chem. *276*, 44488–44494.

Isaacs, R.J., Davies, S.L., Sandri, M.I., Redwood, C., Wells, N.J., and Hickson, I.D. (1998). Physiological regulation of eukaryotic topoisomerase II. Biochim. Biophys. Acta *1400*, 121–137.

Ishida, R., Miki, T., Narita, T., Yui, R., Sato, M., Utsumi, K.R., Tanabe, K., and Andoh, T. (1991). Inhibition of intracellular topoisomerase II by antitumor bis(2,6-dioxopiperazine) derivatives: mode of cell growth inhibition distinct from that of cleavable complex-forming type inhibitors. Cancer Res. *51*, 4909–4916.

Jensen, P.B., Sorensen, B.S., Demant, E.J., Sehested, M., Jensen, P.S., Vindelov, L., and Hansen, H.H. (1990). Antagonistic effect of aclarubicin on the cytotoxicity of etoposide and 4′-(9-acridinylamino)methanesulfon-*m*-anisidide in human small cell lung cancer cell lines and on topoisomerase II-mediated DNA cleavage. Cancer Res. *50*, 3311–3316.

Jensen, L.H., Dejligbjerg, M., Hansen, L.T., Grauslund, M., Jensen, P.B., and Sehested, M. (2004). Characterisation of cytotoxicity and DNA damage induced by the topoisomerase II-directed bisdioxopiperazine anti-cancer agent ICRF-187 (dexrazoxane) in yeast and mammalian cells. BMC Pharmacol. *4*, 31.

Jensen, L.H., Thougaard, A.V., Grauslund, M., Sokilde, B., Carstensen, E.V., Dvinge, H.K., Scudiero, D.A., Jensen, P.B., Shoemaker, R.H., and Sehested, M. (2005). Substituted purine analogues define a novel structural class of catalytic topoisomerase II inhibitors. Cancer Res. *65*, 7470–7477.

Ju, B.G., Lunyak, V.V., Perissi, V., Garcia-Bassets, I., Rose, D.W., Glass, C.K., and Rosenfeld, M.G. (2006). A topoisomerase IIβ-mediated dsDNA break required for regulated transcription. Science *312*, 1798–1802.

Kanoh, N., Honda, K., Simizu, S., Muroi, M., and Osada, H. (2005). Photo-cross-linked small-molecule affinity matrix for facilitating forward and reverse chemical genetics. Angew. Chem. Int. Ed. Engl. *44*, 3559–3562.

Kawatani, M., Okumura, H., Honda, K., Kanoh, N., Muroi, M., Dohmae, N., Takami, M., Kitagawa, M., Futamura, Y., Imoto, M., et al. (2008). The identification of an osteoclastogenesis inhibitor through the inhibition of glyoxalase I. Proc. Natl. Acad. Sci. USA *105*, 11691–11696.

Kimura, S., Ito, C., Jyoko, N., Segawa, H., Kuroda, J., Okada, M., Adachi, S., Nakahata, T., Yuasa, T., Filho, V.C., et al. (2005). Inhibition of leukemic cell

 ©2011 Elsevier Ltd All rights reserved